REGIME MAPPING AND THE ROLE OF THE INTERMEDIATE REGION IN WALL-COATED MICROREACTORS

J. P. Lopes[1,*], M. A. Alves[2], M. S. N. Oliveira[3], S. S. S. Cardoso[4] and A. E. Rodrigues[1]

[1] Laboratory of Separation and Reaction Engineering, Associate Laboratory LSRE/LCM, University of Porto, Rua Dr. Roberto Frias s/n, 4200-465 Porto, Portugal

[2] Transport Phenomena Research Center (CEFT), Department of Chemical Engineering, University of Porto, Rua Dr. Roberto Frias s/n, 4200-465 Porto, Portugal

[3] Department of Mechanical and Aerospace Engineering, University of Strathclyde, Glasgow G1 1XJ, UK

[4] Department of Chemical Engineering and Biotechnology, University of Cambridge, New Museums Site, Pembroke Street, Cambridge, CB2 3RA, UK

*Corresponding author. J. P. Lopes. Tel.: +351 22 508 1578. E-mail: jplopes@fe.up.pt

ABSTRACT

Operation of a wall-coated microreactor can occur in several mass transfer-reaction regimes. We define these regimes analytically in several planes of a multi-parametric map, taking into account the different degrees of concentration profile development, as well as the influence of non-unity orders of reaction and reactant inhibition in the kinetic law. It was found that the regions where conversion can be calculated from simplified mass transfer models are not discriminated by common results for entrance-length. We also illustrate the trade-offs that exist across this operating map concerning the catalyst design (costs associated with loading and volume) and overall system performance (evaluated in terms of reactant conversion, flow efficiency and microreactor effectiveness). It is shown that under certain conditions, the existence of moderate mass transfer resistance can be advantageous (even if internal limitations cannot be avoided), clarifying the role of the intermediate transport-reaction region.

KEYWORDS

Microreactor; Regime mapping; Development length; Mass transfer; Reaction engineering; Catalysis

1 INTRODUCTION

Microchannels with reactive walls can be found in many applications in the fields of energy generation (Karakaya et al., 2009; Kolb et al., 2004), environmental protection (Hernández Carucci et al., 2009), synthesis of fine chemicals (Tadepalli et al., 2007) and biotransformations (Fu et al., 2012). They can appear as microfabricated wall-coated channels or as washcoated monoliths. The behavior of these heterogeneous systems is mainly determined by the following mechanisms: convection in single phase channel flow, diffusion towards the walls and inside the coating, and reaction in the catalyst. Even though the complete mathematical model can be solved numerically, the insight brought about by an analytical analysis usually requires the reduction of the full problem to simplified limits, where only some of the aforementioned

mechanisms are considered important in a first approximation (Figure 1). This simplification is useful for several reasons: (*a*) simplified models are amenable to analytical solution (allowing explicit parametric dependence; kinetic and shape normalizations, etc.), (*b*) real-time simulation, optimization and control applications require computationally cheap models; (*c*) pseudo-homogeneous models are desirable for kinetic measurements (Berger and Kapteijn, 2007a; Groppi et al., 2001; Salmi et al., 2013), and (*d*) controlling limits are often pointed out as the regimes of interest.

The latter point can be in some aspects debatable. First, it is widely stated that operating at the microscale has several advantages, namely the enhanced heat and mass transfer due to the large surface-to-volume ratio, and the use of thin coatings as a way to efficiently use the catalyst volume. In fact, microreactors have been used as kinetic devices for many years now (Cao et al., 2007). In addition, microreactor design in kinetic control has been proposed in wall-coated channels (Fukuda et al., 2012). However, evidence of internal, as well as external, mass transfer limitations exist. Actually, the timescale of a (pseudo) homogeneous reaction does not depend on the channel characteristic length (Renken and Kiwi-Minsker, 2008), whereas the characteristic time for wall-catalyzed reactions is proportional to this dimension, hence benefiting from miniaturization. Thus, fast, high temperature heterogeneous reactions are highlighted as the main candidates for microprocessing and several systems operating under "harsh" conditions, with explosive behavior, or within the concept of "new windows of operation" are currently under study (Hessel et al., 2011).

Even though these limits are of interest, their description of the operation at the microscale is incomplete, since in many practical cases: (*i*) wall concentration annulment (defining mass transfer control in the reaction-transport competition) may be attained only for very high temperatures, catalyst activities, etc., (*ii*) kinetic conditions require longer channels to attain specified conversion values (Gonzo et al. (2011) indicate this as the reason why most washcoats in monolith reactors operate in the intermediate regime with effectiveness factors between 0.4 and 0.8), and (*iii*) at the microscale, the entrance length of the concentration profile (resulting from the convection-diffusion balance) cannot be neglected, similarly to what happens in heat transfer (Alfieri et al., 2012; Rosa et al., 2009). Moreover, Wijngaarden, Kronberg and Westerterp (1998) remarked that the economically feasible range for the effectiveness factor in industrial catalytic reactors would be between 0.7 and 0.9, taking into account both investment (higher reactor volume) and compression (higher pressure drop) costs. Therefore, in many situations, operation falls into the intermediate region of influence of convection-diffusion-reaction mechanisms and, as we show in this paper, this may be desirable. Recently, more complete descriptions of this problem have been presented (see Table 1). The delimitation of the intermediate region by the boundaries for the limiting models was also accomplished analytically for linear and nonlinear kinetics (Lopes et al., 2012c). Moreover, temperature diagrams for linear kinetics were calculated numerically (Joshi et al., 2010). However, there are

still many open questions in this analysis and the purpose of this work is to clarify them. Namely:

(1) The applicability ranges of simplified mass transfer models in the convection-diffusion spectrum are not correctly predicted from the known results for the entrance length. Their validity is properly determined in section 3, derived from a uniformly valid solution.

(2) The behavior of the system composed by the microchannel and catalyst layer is described at least by 4 dimensionless parameters, as shown in section 2. In previous literature, only some planes of this multi-dimensional operating space were considered. In section 4, we highlight the effects of kinetic nonlinearities and the relative importance of internal and external phenomena in the design of the catalyst layer.

(3) The design of microchannels is based on criteria with conflicting outcomes (as discussed above). In section 5, design evaluation in the presence of a constraint on conversion and existing trade-offs are discussed.

2 DESIGN PARAMETERS IN A MICROCHANNEL REACTOR

It is possible to reduce the design of an isothermal coated microchannel (Figure 2) to four independent dimensionless parameters:

(*a*) the Graetz number (including the operation flow rate and the channel length, which normalizes the axial distance z and appears in the aspect ratio $\alpha = a / L$),

$$\frac{\alpha\, Pe_m}{z} = \frac{a^2 \langle u \rangle}{z\, L\, D} \tag{1}$$

(*b*) the inlet Damköhler number (with the characteristic radius of the channel a and reaction rate referred to the inlet concentration and temperature per fluid-solid interface area, $\hat{R}_{surf}$),

$$Da_{in} = \frac{a}{D} \frac{\hat{R}_{surf}\left(\hat{c}_{in}\right)}{\hat{c}_{in}} \tag{2}$$

(*c*) a 'diffusion ratio' (where the diffusivities and length scales of both domains are compared),

$$\Delta = \frac{D_{eff}\, a}{t_w\, D} \tag{3}$$

(*d*) and a parameter related to the catalyst geometry, namely the ratio between the volume, surface and thickness of the coating:

$$\upsilon = \frac{V_{cat}}{t_w\, S_{surf}}. \tag{4}$$

Note that for an annular coating $\upsilon = 1 + t_w/(2a)$. The geometry of the channel cross-section is accounted for using a shape factor S (equals 1 for circular channel, 0 for slit). A parameter related with channel shape and flow profile also appears:

$$\sigma_C = \frac{u_{\max}}{\langle u \rangle} \frac{a\, S_{surf}}{V_{ch}} = \frac{u_{\max}}{\langle u \rangle} (S+1). \tag{5}$$

It can be interpreted as the ratio between the maximum and the actual flowrate in channels with the same wall area S_{surf} and transverse characteristic dimension a (equals 1 for plug-flow between parallel plates). The parameter σ_C increases with curvature and with laminar velocity profile development. Conversion also increases with σ_C for the same value of the Graetz number, Eq.(1).

The Damköhler number Da incorporates internal diffusion effects through the effectiveness factor (η): $Da = Da_{in}\,\eta$, where η is a function of the other dimensionless numbers. Hence, Da is not independent from the parameter set given above and should be used instead of Da_{in}, whenever convenient. The aspect ratio of the channel ($\alpha = a/L$) governs the importance of axial diffusion with respect to the transverse one. This ratio is typically very small to guarantee small dispersion and for fabrication convenience. When compared with convection, axial diffusion is important only in the vicinity of the inlet, in a region of length $\hat{z} \sim O(a/Pe_m)$, which under the typical conditions considered here is negligible. Thus, Eq.(1) will represent the dimensionless length. The Graetz number can be related directly to the dimensionless pressure drop (Euler number) by the Darcy–Weisbach equation in laminar conditions (with the geometry dependent friction factor coefficient $C_D = f_D\, Re$ and Schmidt number $Sc = \nu/D$):

$$\Delta P = \frac{\Delta \hat{P}}{\frac{1}{2}\rho \langle u \rangle^2} = \frac{S+1}{2} C_D\, Sc \frac{z}{\alpha\, Pe_m}. \tag{6}$$

Isothermal conditions are assumed here, and are a good approximation in microreactor arrangements with integrated heat-exchanger functionalities, small channel diameters, and high thermal conductivity materials (Rebrov et al., 2003). The validity of this assumption should be evaluated for particular systems, as discussed in the literature (Norton et al., 2005).

3 CONVERSION WITH DIFFERENT DEGREES OF PROFILE DEVELOPMENT

The analysis of the concentration profile development presented here, has two distinctive features:

(*a*) In general, the development length depends not only on the relative magnitude of convection and transverse diffusion, but also on the rate of the reaction occurring at the wall.

(*b*) Our main purpose is to understand the applicability of mass transfer models (at the entrance-length or for 'long distances') when predicting the reactant conversion profile, given exactly by the series solution (linear kinetics):

$$X_R = 1 - \langle c \rangle = X_{fd} - \sum_{n=2}^{\infty} w_n \exp\left(\frac{-\lambda_n^2\, z}{\alpha\, Pe_{m,\max}} \right). \tag{7}$$

Both the relative errors with respect to the inlet concentration (e) and actual conversion (ε) can be adopted as criteria for the degree of profile development. In particular, choosing:

$$\varepsilon_{fd} = \frac{\left| X_{fd} - X_R \right|}{X_R}, \tag{8a}$$

for fully developed profile, and

$$e_{dev} = \left| X_R - X_{dev} \right|, \tag{8b}$$

for developing profile, seems to yield criteria of comparable strictness. Thus, one can expect results of the form: $z/\alpha Pe_m = f\left(Da, \varepsilon_{fd} \text{ or } e_{dev}\right)$, i.e. dimensionless length as a function of the Damköhler number and the criteria used. This is only possible because an asymptotic expression of the series in (7) was determined (this is summarized in section 3.1, while mathematical details can be found in Supplementary Information).

3.1 Insights into the structure of the conversion profile

By application of an asymptotic technique to (7), we are able to show that the conversion profile is given approximately by

$$X_R = X_{fd}\ \Theta_{fd} + Y_{dev}\ \Theta_{dev}\,. \tag{9}$$

This solution is comparable with Graetz's classical series (7) with several terms (full details in Supp. Info.). The main definitions and asymptotic trends of the terms in (9) are:

- X_{fd} is the fully developed conversion, given in Table 1;
- Θ_{fd} is a weighting function which accounts for the importance of X_{fd} and behaves like:

$$\Theta_{fd} \sim \frac{\lambda_1^2}{1-w_1}\frac{z}{\alpha Pe_m} \sim \begin{cases} \dfrac{1}{Da}\dfrac{z}{\alpha Pe_m} & \text{as } Da \to 0 \\ \dfrac{z}{\alpha Pe_m} \to 0 & \text{as } Da \to \infty \end{cases}, \qquad \text{when } \frac{z}{\alpha Pe_m} \to 0 \tag{10a}$$

$$\Theta_{fd} \to 1 - \left(1 - w_{1,\infty}\right)\left(\frac{Da}{1+Da}\right)e^{-\lambda_2^2 z/\alpha Pe_m} \to 1, \qquad \text{when } \frac{z}{\alpha Pe_m} \to \infty\,. \tag{10b}$$

  Since $0 < \Theta_{fd} < 1$, the fully developed asymptote dominates at large dimensionless distances for all values of Da (deviation from 1 in (10b) is exponentially small). *Surprisingly, this dominance may also occur near the inlet provided that* $Da = O\left(z/\alpha Pe_m\right)$, *in the asymptotic sense (i.e.* Da *is not much higher than* $z/\alpha Pe_m$*).*

- Y_{dev} is associated with developing features of the concentration profile and presents two main behaviors:

$$Y_{dev} \sim O\left[\left(z/\alpha Pe_m\right)^{(\beta-1)/2}\right] \sim \begin{cases} Da^2\left(z/\alpha Pe_m\right)^{3/2} & , Da \le Da_T \\ \rightarrow X_{dev} = O\left[\left(z/\alpha Pe_m\right)^{1-q}\right], & Da > Da_T \end{cases} \quad (11)$$

The function $\beta\left(Da\right) \simeq \left(\beta_0 + \beta_\infty\, Da\right)/\left(1+Da\right)$ decreases from $\beta_0 = 4$ to β_∞ ($= 7/3$ for laminar flow, see Supp. Info.). To understand how Y_{dev} unfolds into two different forms, for each range of Da, the inlet region must be considered. The limit of (9) as $z/\alpha Pe_m \rightarrow 0$ is:

$$X_R \simeq Y_{dev} + f\left(Da\right)\frac{z}{\alpha\, Pe_{m,\max}} \quad (12)$$

According to (11), Y_{dev} is the leading-order term in (12) only if $\beta < 3$ (corresponding to $Da > Da_T = 1.5$). Otherwise the $f\left(Da\right)$ term, which includes information from both asymptotes, dominates. *The contribution of Y_{dev} to the profile at the inlet changes from a minor term when $Da \le Da_T$, to a full representation of conversion as $Da \rightarrow \infty$.* In this latter case, both contributions (X_{fd} and X_{dev}, given in Table 1) become completely separable.

- Θ_{dev} weighs the importance of Y_{dev}, with the following trends:

$$\frac{z}{\alpha Pe_m} \rightarrow 0:\ \Theta_{dev} \sim 1 - A\left(\frac{z}{\alpha\, Pe_m}\right)^{(3-\beta)/2} \sim \begin{cases} -\sqrt{\alpha\, Pe_m/z} & \text{as } Da < Da_T \\ 1 & \text{as } Da > Da_T \end{cases} \quad (13a)$$

$$\frac{z}{\alpha Pe_m} \rightarrow \infty:\ \Theta_{dev} \rightarrow \exp\left(-\lambda_2^2\, z/\alpha Pe_{m,\max}\right) \rightarrow 0\,. \quad (13b)$$

The contribution of the developing profile dominates the inlet for $Da > Da_T$, represents a small correction $\Theta_{dev}\, Y_{dev} \sim O\left\lfloor Da^2\left(z/\alpha Pe_m\right)\right\rfloor$ for entrance-length at lower reaction rates and disappears as the distance increases. Correct values, e.g. of $A\,(>0)$, are given in Supp. Info.

Regarding the structure of the conversion profile described above, it is worth emphasizing:

(a) Both mass transfer models yield the same first estimate at the kinetically controlled channel inlet ($X_{fd} = X_{dev} \sim Da\, z/\alpha Pe_m$). Distinguishable higher-order terms from X_{fd} are of $O\left\lfloor Da\left(z/\alpha Pe_m\right)^2\right\rfloor$, while the ones from $\Theta_{dev}\, Y_{dev}$ are of $O\left(Da^2\, z/\alpha Pe_m\right)$. Hence, development of this profile increases with $\left(z/\alpha Pe_m\right)/Da$.

(b) For long distances in a kinetically controlled channel, expansion of X_{fd} for $Da < \alpha Pe_m/z \rightarrow 0$ coincides with the same limit of X_{dev}. Moreover, the correction due to

$Y_{dev}\Theta_{dev}$ is much larger than the second exponential term of the series as $z/\alpha Pe_m$ increases (see (11) and (13b)).

The result from these two effects is an *overlapping region*, which increases as $Da \to 0$. This corresponds to a scenario where slow reactant consumption is insufficient to generate appreciable concentration gradients, and therefore the fully developed and boundary layer descriptions agree. On the other hand, under mass transfer control, developed and entry-length regions of the concentration profile are separable contributions in (9), leading to the appearance of a *transition region.*

3.2 Fully developed profile boundary

(a) Mass transfer control

The dimensionless channel length (reciprocal of the Graetz number) required for profile development within an error e_{fd} is quite insensitive to Damköhler number near the *mass transfer controlled regime* [see Eq.(10b)]. Therefore, the uniformly approximation when the boundary condition approaches Dirichlet type is valid and it predicts:

$$\frac{z}{\alpha Pe_{m,\max}} = \frac{1}{\lambda_{2,\infty}^2} \ln\left(\frac{1-w_{1,\infty}}{e_{fd}}\right). \qquad (Da \to \infty,\ Da > Da_T) \qquad (14)$$

Note that shape dependent $w_{1,\infty}$ and $\lambda_{1,\infty}$ are calculated in Lopes et al. (2012a; 2011b) (estimations have also been given) and that $\lambda_{2,\infty} = \lambda_{1,\infty} + \Delta\lambda$, where $\Delta\lambda = 4$ for laminar flow as detailed in Supp. Info.

If conversion can be calculated from a fully developed mass transfer controlled model with error e_{fd} (given by Eq.(14)), then the minimum predictable conversion is

$$X_R = 1 - w_1 \left(\frac{e_{fd}}{1-w_{1,\infty}}\right)^{\frac{\lambda_1^2}{\lambda_{2,\infty}^2}}. \qquad (15)$$

Near the mass transfer controlled limit (Lopes et al., 2011b): $w_1 \to w_{1,\infty}$ and $\lambda_{1,\infty}^2/\lambda_{2,\infty}^2 = (1+\Delta\lambda/\lambda_{1,\infty})^{-2} = O(0.01-0.1)$. Naturally, $\varepsilon_{fd} \to 0$ only when $X_R \to 1$. In terms of the relative error ε_{fd}, an improved version of Eq.(14) can be obtained as

$$\frac{z}{\alpha Pe_{m,\max}} = \frac{1}{\lambda_{2,\infty}^2} \ln\left(\frac{1-w_{1,\infty}}{\varepsilon_{fd}}\right) - \frac{1}{\lambda_{2,\infty}^2} \ln\left[1 - w_{1,\infty}\left(\frac{\varepsilon_{fd}}{1-w_{1,\infty}}\right)^{(1+\Delta\lambda/\lambda_{1,\infty})^{-2}}\right]. \qquad (16)$$

The first term is dominant, while in the second, a simplification is admissible at high conversion: $e_{fd} \sim \varepsilon_{fd}$.

(b) Kinetic control

As noted previously, the validity of the fully developed profile increases as Da decreases (towards *kinetic control*) more significantly than the reciprocal of Graetz parameter. Thus, the deviation can be represented by the second term in Graetz series:

$$e_{fd} = w_{2,0} \exp\left(-\frac{\Delta\lambda^2 \, z}{\alpha Pe_{m,\max}} \right) \sim w_{2,0} . \qquad (Da \to 0) \qquad (17)$$

The last simplification eliminates the dependence on Graetz parameter and is reasonable since the boundary moves towards $z/\alpha Pe_m \to 0$ as $Da \to 0$. In Supp. Info., we postulate how the weights w_n in Eq.(7) depend on the respective eigenvalues λ_n for $n > 1$. An order of magnitude estimate can be obtained using this information:

$$e_{fd} = \frac{w_{1,0} \, \lambda_{1,0}^4}{(\lambda_{1,0} + \Delta\lambda)^4} \simeq \frac{\sigma_C^2 \, Da^2}{(\Delta\lambda)^4} .$$

The relative error ε_{fd} is obtained using the leading-order term ($X_R \simeq \sigma_C \, Da \, z/\alpha Pe_{m,\max}$),

$$\frac{z}{\alpha Pe_{m,\max}} = \frac{S+3}{S+1} \frac{Da}{(\Delta\lambda)^4 \, \varepsilon_{fd}} . \qquad (18)$$

The correction applied to the numerical coefficient in (18) was tested for both circular and planar geometries in a meaningful range of Da values. The minimum conversion that can be estimated from this limit model near kinetic control is

$$X_R \simeq \frac{(S+3)^2}{2(\Delta\lambda)^4} \frac{Da^2}{\varepsilon_{fd}} .$$

For $X_R < 1$, a constraint on the maximum value specified for Da exists.

(c) Correlation for all reaction rates

Both asymptotes [Eqs.(14) and (18)] can be combined in a general expression:

$$\frac{\alpha Pe_{m,\max}}{z} = \frac{S+1}{S+3} \frac{(\Delta\lambda)^4 \, \varepsilon_{fd}}{Da} + \frac{\lambda_{2,\infty}^2}{\ln\left[(1 - w_{1,\infty})/\varepsilon_{fd} \right]} \qquad (19)$$

The last term in (19) can be replaced by the reciprocal of (16). Eq.(19) is plotted in Figure 3 for several values of ε_{fd} .

3.3 Developing profile boundary

(a) Mass transfer control

Near *mass transfer control*, the deviation can be calculated by using an additional term in the so called extended Lévêque solutions (Shah and London, 1978),

$$\frac{z}{\alpha\, Pe_{m,\max}} = \frac{e_{dev}}{A}\,.$$

According to the results for laminar flow (Shah and London, 1978): $A = 2.4$ in circular microchannels, while $A = 0.15$ for microslits. For fast linear kinetics, we follow the analysis in Lopes et al. (2011b) to show that:

$$e_{dev} = \frac{A\, z}{\alpha\, Pe_{m,\max}}\left[1 - \frac{B}{Da}\left(\frac{\alpha Pe_{m,\max}}{z}\right)^{q}\right]. \tag{20}$$

The remaining numerical coefficients are: $B = 4/\sqrt{\pi}$ and $q = 1/2$ for plug-flow in a circular channel; and $B = 2.035$ and $q = 1/3$ for laminar flow (round tubes and slits). An approximate explicit expression for the Graetz parameter can be obtained from (20) for $Da\, e_{dev}^{q} >> 1$:

$$\frac{z}{\alpha\, Pe_{m,\max}} = \frac{e_{dev}}{A}\left[1 + \frac{B}{Da}\left(\frac{A}{e_{dev}}\right)^{q}\right]. \tag{21}$$

Eq.(21) was found to work very reasonably even near the transition range ($Da \sim 1$), as shown in Figure 4b, where for $e_{dev} = 0.1\%$, predictions at high and low Da overlap. The maximum conversion obtained from this model is

$$X_{dev} = \frac{N}{A^{2/3}}\left[1 + \frac{B}{Da}\left(\frac{A}{e_{dev}}\right)^{q}\right]^{2/3} e_{dev}^{2/3} \simeq \frac{N}{A^{2/3}}\, e_{dev}^{2/3}\,, \tag{22}$$

where $N = 3^{4/3}\left(S+1\right)\left(S+3\right)/\left\lfloor 2^{5/3}\,\Gamma(1/3)\right\rfloor$ is taken from Lévêque's solution with Dirichlet boundary condition.

(b) Kinetic control

The applicability boundary under *kinetic control* is less straightforward. Note that since the developing profile may describe results at high values of $z/\alpha Pe_m$, extended Lévêque series (for short distances) are not applicable. Here, our uniformly valid solution is of interest. The limit of Eq.(9) for low Damköhler number, and small Graetz parameter, is given by

$$X_R \simeq \frac{\sigma_C\, Da\, z}{\alpha\, Pe_{m,\max}} - \left[\frac{1}{2}\left(\frac{\sigma_C\, z}{\alpha\, Pe_{m,\max}}\right)^{2} + \left(\frac{1+S}{Sh_{fd,0}}\right)\frac{z}{\alpha\, Pe_{m,\max}} - \left(\frac{1+S}{Sh_{fd,0}}\right)^{2}\right] Da^{2} + \ldots\,. \tag{23}$$

Since the leading term is the result from our approximate correlation (and Lévêque's solution) in the limit of small Da, and the first term in brackets is dominant for $z/\alpha Pe_m >> 1$:

$$\frac{z}{\alpha\, Pe_{m,\max}} = \frac{\sqrt{2}}{\sigma_C}\frac{\sqrt{e_{dev}}}{Da} = \frac{2}{\sigma_C\, Da}\frac{\varepsilon_{dev}}{1+\varepsilon_{dev}}. \qquad (24)$$

The maximum predicted conversion is $X_R \simeq \sqrt{2\, e_{dev}} \simeq 2\, \varepsilon_{dev}$.

3.4 Validity of mass transfer models

The quality of the conversion prediction by each limiting model is illustrated in Figure 5. The boundaries defined earlier for given values of ε_{fd} and e_{dev}, establish the following picture: two areas where only one model is able to represent X_R with the required accuracy exist near the Dirichlet limit, separated by a *transition region* (no satisfactory model). As the Damköhler number decreases, the range of this region decreases, until it is reduced to a single point. For lower values of Da, an *overlapping region* (both models are suitable) appears and increases as $Da \to 0$. Figure 5 (b) shows these validity ranges for 3 qualitative behaviors (transition in region of finite length, transition in a single point, and overlapping region of finite length) in terms of the observable conversion as a function of the dimensionless distance (limiting models were calculated analytically according to Lopes et al. (2011b)).

This understanding seems to be at odds with previous literature, namely: (*i*) the overlapping region in Figure 5a has not been recognized before, and (*ii*) the entrance length (where $Sh \geq 1.05\, Sh_{fd}$) decreases with Da, with a 30-45% reduction for uniform wall concentration relative to the uniform flux asymptote (Shah and London, 1978), in apparent contradiction with e.g. Figure 3. The following additional remarks should be made:

1. The definition of the entrance length in classical literature is mostly based on a (arbitrarily defined) margin for an increase in Sherwood (or Nusselt) number compared to the fully developed value. Lopes et al. (2011a) obtained the same quantities by intersection of the fully developed and developing asymptotes of Sh. This information does not contemplate a transition (or overlapping) region, predicts an increase in the entrance-length as Da decreases, and is directed towards the selection of models for Sherwood number in the analysis of the mass transfer resistances. Here, however, we are interested in analyzing the suitability of *conversion* calculation from two-dimensional models.

2. Our conclusions are in agreement with other studies in the literature. Lopes et al. (2011b) showed that the error in estimating conversion with one term in Graetz series when $\alpha\, Pe_m/z$ increases is more significant for high values of Da. Gervais and Jensen (2006) concluded that the importance of the fully developed description increases when $Da \to 0$, comparing simplified models with the numerical solution. They showed that terms in Graetz series (7), other than the first, decay much faster for lower Da, and this results in a reduction of the absolute error of the fully developed asymptote by one order-of-magnitude at the inlet. This is also observed in the analysis in Supp. Info.

3. Results in sections 3.2 and 3.3 provide the applicability ranges for simplified mass transfer models, explicit on relative errors and for the general case of a wall reaction with any rate. Expressions like these have not been reported, in particular for the case of Robin boundary conditions (finite thermal resistance in the heat transfer problem). Moreover, it is also recognized (Gervais and Jensen, 2006) that the critical value of Graetz's number at which Lévêque's model is no longer satisfactory cannot be determined from a straightforward approach when Da is finite, and that the required numerical evaluation is tedious.

Since the Graetz problem has been formulated for several geometries (with the calculation of the several coefficients that appear), the results in this section can be applied to shapes other than slit and circular channels. Concerning the use of these results when the flow is also developing, e.g. in the most unfavorable case (Dirichlet boundary condition), we refer to Shah and London (1978) which conclude that the value presented for the thermal entrance length including simultaneously developing flow is a weak function of $Pr\,[\text{or } Sc] \geq 0.7$. Hence the validity ranges in the lower practical range of Sc number can be reasonably described by the fully developed laminar asymptote. Another straightforward application of our results is for a flat velocity profile which yields an approximation as $Sc \to 0$.

4 REGIME MAPPING

Our approach uses the degree of mass transfer control (θ) and the effectiveness factor (η) as regime definers,

$$\theta = \frac{Da}{Sh + Da} = \frac{\langle c \rangle - c_{surf}}{\langle c \rangle - c_{surf} + R\left(c_{surf}\right)} \tag{25}$$

$$\eta = \frac{\iint R\left(c_{cat}\right) dA_{cat}}{R\left(c_{surf}\right) A_{cat}}. \tag{26}$$

Consider the isothermal decomposition of a single reactant, with a reaction rate expressed per volume of catalyst by: $\hat{R}_V\left(\hat{c}_w\right)=k\,\hat{c}_w^m\left(1+\hat{c}_w\,k'/\hat{c}_{in}\right)^{-p}$. The dimensionless reaction rate (referred to inlet conditions) is

$$R(c)=\frac{\hat{R}_V\left(\hat{c}\right)}{\hat{R}_V\left(\hat{c}_{in}\right)}=\frac{(1+k')^p\,c^m}{(1+k'\,c)^p}\,. \tag{27}$$

Assigning sensible values to θ and η (as strict as desired) identifies *overall regimes* (in the sense that both channel and catalyst present the same level of mass transfer resistance). It was found (Lopes et al., 2012c) that the controlling phenomena changes when a certain value of the diffusion ratio is attained (Δ^*). The existence of regimes where mass transfer control is observed more significantly in one phase is also related with this parameter. Thus, regimes of *intra-* and *inter-phase* mass transfer control (where the most important resistance is concentrated exclusively in one phase) are also considered.

The dimensionless quantities presented in section 2 form a multi-parametric space, where the behavior of a given system (combination of design and operation of both microchannel and catalyst) is described by a single point. To reduce the problem so that graphical representation is possible, we consider several "slices" of this parametric space, where we represent the boundary surfaces for the different regimes. Table 2 shows the expressions for these boundaries, which generalize previous work (Lopes et al., 2012c).

The results are shape normalized regarding the channel and catalytic layer cross-sections. Namely, the Sherwood number can be found in the literature for several geometries and suitable boundary conditions with axially and/or peripherally uniform flux or concentration (Shah and London, 1978). The formulation for the effectiveness factor was derived from a generic model (Lopes et al., 2012b), which contains a shape factor that can be fitted to the actual geometry (several examples for catalytic pellets exist (Mariani et al., 2008; Mocciaro et al., 2011)). In its simplest form this is related to the ratio of catalyst volume per surface area and thickness (parameter υ given in Eq.(4)). For nonuniform coatings, an improvement to the numerical procedure conceived by Papadias et al. (2000) was given in Lopes et al. (2012b) Since these factors account explicitly for the effect of shape, this methodology is able to compare different geometries in a straightforward manner.

At this point, we recall that previous works regarding regime mapping (e.g. Joshi et al. (2010)) are associated with the following drawbacks: (i) dimensional formulation, requiring a number of variables to remain fixed, while a selected design or operation feature is varied in a limited range; (ii) repetitive numerical solution of the problem at both channel and catalyst scales whenever any condition or criterion is admitted to change from base case values; (iii) inability to distinguish between regimes with overall or localized mass transfer limitation; (iv) inability to a priori identify the domain most afflicted by resistance; (v) incapacity to reflect any consequence introduced by the nonlinearity in the kinetic law.

On the contrary, we remark the superiority of the approach presented in Table 2: (i) analytical results, achieving parametric dependence; (ii) generalized treatment for any description of external or internal mass transfer; (iii) ability to capture nonlinear kinetic effects and the relative importance of internal to external resistance; and (iv) accuracy compared to 2D numerical calculations, and respect of the theoretical asymptotes. Hence, the comprehensive picture of the system behavior can be obtained effortlessly.

4.1 Intermediate reaction-transport region

The intermediate region can be delimitated with respect to the relative magnitude of the reaction rate (boundaries given in Table 2), as well as to the degree of profile development (results from section 3). This is shown in a $Da_{in} - \alpha\, Pe_m/z$ plot (Figure 6) for linear kinetics in an annular coating with $\upsilon = 1.05$ and for two values of the diffusion ratio (fully developed laminar flow).

The dependency of the fully developed and developing boundaries in Figure 6 on the diffusion ratio results from the fact that these were expressed in terms of $Da = \eta\, Da_{in}$ in section 3. To achieve the representation in terms of Da_{in}, the effectiveness factor is calculated by the analytical solution found in Lopes et al. (2012b). Then, since previous results are written explicitly for $\alpha\, Pe_m/z$, the nonlinear $\eta(Da_{in})$ function is easily evaluated for given values of Da_{in}.

The superposition of the reaction-transport and profile development analyzes leads to the identification of an intermediate region (the area in the diagram outside previously defined boundaries). We characterize 5 particular points (vertices) defining this area.

High conversion vertex, V_1

If Da_{in} and $\alpha\, Pe_m/z$ are the coordinates of V_1 (given by Eqs.(14) and (T5)), then for higher Damköhler number and lower Graetz parameter, the concentration profile can be considered fully developed and mass transfer controlled. An appropriate mass transfer model consists in the first term of Graetz series (7) with eigenvalue and integration constant evaluated at Dirichlet conditions (tabulated values for several geometries exist (Kays and Crawford, 1980; Shah and London, 1978)). Physically, this may correspond to a long microchannel with a fast reaction occurring at the wall, so both reaction and transverse diffusion dominate. This region is associated with high reactant conversion. The minimum conversion, at the vertex in Figure 6, can be calculated from Eq.(15): $X_R = 1 - w_{1,\infty}\left[\varepsilon_{fd}/(1-w_{1,\infty})\right]^{\lambda_{1,\infty}^2/\lambda_{2,\infty}^2} = 0.49$ (also in agreement with Figure 5a). Note that this value is nearly insensitive to the criterion for mass transfer control, θ.

Hot inlet vertex, V_2

The regime delimitated by the boundaries intersecting at V_2 is characterized by significant energetic requirements to attain mass transfer control (which increase in developing conditions) and energy dissipation rates associated with high fluid velocities. The reduced residence time in a short channel or at the inlet section penalizes conversion (in the conditions of Figure 6 and according to Eq.(22): $X_R \le N\left(e_{dev}/A\right)^{2/3} = 0.105$, see also Figure 5a). The profile is mass transfer controlled but developing, thus Lévêque's solution with constant wall temperature is appropriate. This may represent the state of the inlet section of a channel attaining high conversion at its exit.

When determining the boundary for overall mass transfer control, we have used the value of Sherwood number evaluated with Dirichlet wall conditions (corresponding to low surface concentrations, required to achieve values of θ close to 1). However, the correlation for Sherwood number presented in Table 1 has two independent terms, and other forms namely for the developing term may be introduced if desired (e.g. accounting for axial diffusive transport). In order to ascertain the adequacy of the asymptote of Sh_{dev} with Dirichlet boundary condition, we compare the analytical predictions from Eq.(T5) with the numerical simulation of a 2D model, where the generic Robin condition was implemented at the wall and the axial diffusion term retained. This is shown in a $Da_{in} - \alpha Pe_m/z$ map in Figure 7, where regions of overall mass transfer control ($\theta \ge 0.90$) and mixed control ($\theta < 0.90$) can be depicted. The following observations should be made: (a) the regime boundary predicted using the Dirichlet condition is suitable to describe these numerical results; (b) the range of the dimensionless axial distance covered by this picture is wide enough (including the near-inlet region) to describe meaningful conversion in channels with small aspect ratio ($\alpha \to 0$); (c) the variation in the values of θ is very weak in this parametric area, and minor differences are observed from the values of Da_{in} predicted using the Neumann boundary condition; and (d) adopting a conservative (lower) solution is a design best practice. For all these reasons, we find the Dirichlet boundary condition suitable for our analysis.

Middle point, V_3

The intersection of boundaries for fully developed and developing profiles occurs at values of $Da \sim 1$ (internal control: $\Delta Da_{in} \sim 1$). At this point, convection and diffusion balance. A conservative criterion for transition between mass transfer models when $Da < 1$ is the vertex coordinate. The simplest approximation to this point is given by the intersection of Eqs.(19) and (21), which is very close to the full development length at Dirichlet conditions, Eq.(14). The

intermediate region appears centered around this point with respect to both profile development (east and west semi-planes) and mass transfer control (north and south semi-planes).

Low conversion vertex, V_4

The region in Figure 6 for high Graetz parameter and low Damköhler number delimits an 'inlet' region, in the sense that conversion is low and dominated by convection. High power dissipation is obtained at high flowrates. Conversion at V_4 is the maximum observed in this regime and is given by ($\varepsilon_{fd} \to 0$):

$$X_R \simeq \left[\frac{(S+3)}{(\Delta\lambda)^2} \frac{\upsilon}{\Lambda} \frac{\Delta}{K_0} \frac{\eta(1-\eta)}{\sqrt{2\,\varepsilon_{fd}}} \right]^2 \sim \frac{\Delta^2 (1-\eta)^2}{\varepsilon_{fd}} \qquad \text{if } \Delta < \Delta^* \ (\eta \to 1), \tag{28a}$$

$$X_R \simeq \frac{(S+3)^2}{2(\Delta\lambda)^4\,\varepsilon_{fd}} \left(\frac{\theta}{1-\theta} Sh_0 \right)^2 \sim \frac{\theta^2}{\varepsilon_{fd}} \qquad \text{if } \Delta > \Delta^* \ (\theta \to 0). \tag{28b}$$

Homogeneous microchannel vertex, V_5

High conversions are possible in kinetic control, for sufficiently long microchannels. In this case, transport is dominated by transverse diffusion, thus high dimensionless pressure drops ($\Delta P \sim L/a^2$) are obtained, Eq.(6). The conversion profile can be estimated by the solution for a homogeneous laminar flow reactor. The minimum conversion attainable in this regime is calculated by $X_R \simeq \sqrt{2\,e_{dev}} \simeq 0.14$ for conditions in Figure 6 and Figure 5a.

Simultaneously developing flow

Microchannel arrangements often include inlet distributors, as barrier pressure drop channels (Al-Rawashdeh et al., 2012) or channel networks (Saber et al., 2010), or uncoated pre-sections, which may develop the inlet velocity profile partially or completely before it reaches the catalytic region. Moreover, in certain conditions (e.g. liquid-phase operation), the flow profile may develop much faster than the concentration profile. On the other hand, the idealized plug-flow may be useful as a limiting case, and can be approached e.g. when measuring intrinsic kinetics using coated microchannels packed with inert glass spheres (Berger and Kapteijn, 2007b; Redlingshöfer et al., 2002). Nevertheless, developing flow from an inlet flat velocity profile can be easily incorporated into our analysis, remembering that the results for mass transfer in the channel are written in terms of Sherwood number and that correlations for this quantity are available as a function of both Graetz and Schmidt number. For example, Shah and London (1978) report such correlations from Churchill and Ozoe (for both Dirichlet and

Neumann conditions at the wall), which work in the relevant range of Sc. One can also consider the developing asymptote derived by the same authors and introduce it into the correlation for Sh in Table 1 as

$$Sh_{dev,\infty} = \frac{0.5642}{\left(1+7.7002\,Sc^{2/3}\right)^{1/4}}\sqrt{\frac{\alpha Pe_m}{z}} \quad \text{or} \quad Sh_{dev,0} = \frac{0.8862}{\left(1+13.2644\,Sc^{2/3}\right)^{1/4}}\sqrt{\frac{\alpha Pe_m}{z}},$$

(Dirichlet or Neumann boundary conditions, respectively) while keeping the same value for $Sh_{fd,\infty}$. Qualitatively, the consequence of this phenomenon is no different from the concentration profile inlet effects considered (enhanced mass transfer towards the coating). In Figure 8, we plot the boundary for overall mass transfer control (according with Eq.(T5), Table 2) for several values of Sc number.

Results from Joshi et al. (2010) are compared with our analytical predictions in Figure 8, after being made dimensionless. It is possible to observe that these system-specific numerical calculations (involving the repetitive solution of partial differential equations for mass transport in channel and catalyst) can be replaced by our simple estimates with all of the previously mentioned advantages. Regarding the mass transfer control boundary, good agreement is observed for $Sc \sim 0.7$ (typical value for air). We also note that under developing conditions, uniform wall flux was assumed by these authors, while uniform wall concentration prevailed downstream. If desired, our correlation for Sh can describe this modeling choice. In our case (small aspect ratio channels), the correlation in Table 1 is appropriate, even near the inlet as shown in Figure 7. Note that the calculation of the kinetically controlled boundary does not require the consideration of the problem at the channel level. Likewise, for overall mass transfer control, the reaction-diffusion problem in the catalyst can be replaced by the diffusional limit of the effectiveness factor, since for the values of Δ considered, the coating is well within this asymptotic regime. Moreover, the data from Joshi et al. (2010) are only a particular case of the results in Table 2 for $\Delta = 0.1-0.2$, $\theta = 0.9$, $\eta = 0.9$, $\upsilon = 1.01$, $m = 1$, $k' = 0$ and $Sc = 0.7$.

4.2 Kinetic nonlinearities in regime mapping

We now consider two effects from the nonlinear concentration dependence of Eq.(27) on regime definition: non unity order of reaction and reactant inhibition. Other aspects such as steady-state multiplicity are not included, but the chemical and diffusional asymptotes are also observed in those situations, and in some cases the 'abnormal' behavior is restricted to the space outside the boundaries. Moreover, provided that a suitable mass transfer correlation is available (several exist in the literature), more complex effects such as simultaneous flow development or non-negligible axial diffusion, can be easily incorporated into this methodology.

In Figure 9a, we plot the inlet Damköhler number as a function of the Graetz (flow) parameter, for a second-order reaction in a circular channel with laminar flow (coated by a thin annular washcoat, $\varepsilon = 0.1$). The parametric areas of the 4 regimes in Table 2 are identified for two values of the diffusion ratio. In Lopes et al. (2012c), we have presented a temperature diagram, which under certain assumptions (namely concerning the temperature dependence of the reaction kinetics and of physical properties) can also be obtained from the dimensionless representation in Figure 9a. Moreover, here we discuss the influence of other parameters (Δ, m and k'), and of the reactant concentration distribution at the channel-coating interface on the different boundaries. Therefore, the description becomes more complete, as we also identify the regions of mixed and interphase kinetic control.

The difficulty which prevents the use of the effectiveness factor in an analytical formulation for nonlinear reactions can be debottlenecked by recognizing the relative importance between internal and external mass transfer resistance. This is governed by the value of Δ compared to Δ^* (given in the first column of Table 2). Hence, if the coating is relatively more afflicted by limitation ($\Delta < \Delta^*$), negligible consumption of reactant in the channel (also near the coating surface) can be assumed in the overall kinetic regime (controlled by the catalyst). The reverse holds if $\Delta > \Delta^*$. For the mass transfer controlled boundary, the diffusional asymptote of the effectiveness factor and the reactant surface distribution near concentration annulment are useful. This introduces a generic dependence on 'external quantities' (Sh_∞ and $\langle c \rangle_\infty$, which are easily evaluated in a spreadsheet software) into Eqs.(T5) and (T6) that disappears if $m = 1$ (first-order reactions). These are nothing but consequences from kinetic nonlinearities (which further couple the internal and external problem). We also note that regimes are mapped in terms of inlet reference (known) conditions, namely Da_{in} (since Da may vary axially for the reasons detailed before).

Overall Kinetic control

For these values of the diffusion ratio Δ, the boundary for kinetic control is given by the value of the inlet Damköhler number so that the effectiveness factor is kept above η (e.g. 0.9). This is the limiting factor, which means that external mass transfer proceeds much faster, and thus reactant is distributed uniformly along the interface at a concentration level very close to the inlet one (conversion in the channel is negligible).

Overall Mass transfer control

The same is not observed under mass transfer control, where the surface distribution of concentration and reaction rates (included in the local Damköhler number for nonlinear kinetics,

referred to surface conditions $\hat{R}_{surf}$ and $\hat{c}_{surf}$) depends on the mass transfer problem in the channel. This yields a distinct area in the diagram, formed by the two boundaries given by Eqs.(T5) and (T6). In particular for low Graetz number, a sharp increase in the required inlet reaction rate is observed. For $m>1$, this happens since the local Damköhler number is decreased by the vanishingly small reaction rate at the fluid-solid interface (severe external mass transfer control). The minimum Damköhler number for overall mass transfer control is obtained at the intersection between both boundaries and is given by

$$Da_{in} = \frac{Sh_\infty\,\theta}{1-\theta}\,\frac{\left(1+\upsilon\left(\upsilon-1\right)\eta\right)^{\frac{2m}{m+1}}}{\eta} \sim \frac{Sh_\infty}{\left(1-\theta\right)\eta} \qquad \text{(for } m>1\text{).} \tag{29}$$

If kinetic laws with $m<1$ are suitable to describe such low surface concentrations, then $\Delta^* \to \infty$ as $\alpha\, Pe_m \to 0$, and the regime is defined by the channel with significant internal limitations (i.e. the effectiveness factor is much smaller than in the linear case). There is also a minimum value of Da_{in} resulting from the increase in concentration (steep decrease of $\langle c \rangle_\infty^{1-1/m}$) and mass transfer coefficient (at a slower rate, included in Sh_∞) as $\alpha\, Pe_m$ increases. In general, one might say that this occurs around the transition region of $\alpha\, Pe_m/z$ values. In this case, it is noticeable how external mass transfer influences the internal problem, since it is well-known that for the same Thiele modulus, effectiveness increases as m decreases.

Interphase mass transfer control

Apart from the previous overall regime (with low wall concentration, but still allowing for strong gradients to develop in the coating), a purely *interphase resistance dominated area* is depicted (where the catalyst may be operating in the intermediate or even kinetic regime). For the parameter values in Figure 9, this behavior is not observed with linear kinetics. This regime appears in the same range where overall mass transfer control is defined by the catalyst, according to Eq.(T6). Hence, it occurs when $m>1$, as suggested by the dependence of Eq.(T10) on $\langle c \rangle_\infty$, for low concentrations.

Intraphase mass transfer control

The two boundaries that delimit the intraphase mass transfer controlled regime intersect at a point, whose coordinates ($\alpha\, Pe_m/z$ and Da_{in}) are determined e.g. by Eq.(T9) and:

$$Sh_0\left(\alpha\, Pe_m/z\right) = \Delta\;\frac{1+\upsilon\left(\upsilon-1\right)\eta}{K_\infty\,\upsilon\,\eta}\;\frac{1-\theta}{\theta} \sim \frac{\Delta}{K_\infty\,\upsilon\,\eta\,\theta}\,. \tag{30}$$

Since this regime is found when $\eta \to 0$ and $\theta \to 0$ (typically K_∞, Δ and υ are $O(1)$), then it is likely that mass transfer ensues in the entrance regime of the microchannel reactor ($\alpha\, Pe_m/z >> 1$). Hence, Eq.(30) yields the minimum value of the Graetz number ($\sim \Delta^3/(\eta\,\theta)^3$) for which this regime can be found at some value of Da_{in}. The region becomes wider as $\alpha\, Pe_m/z$ increases from this value.

Interphase kinetic control and mixed control

When the catalyst coating is comparably more afflicted by diffusional limitations than the channel (i.e. $\Delta < \Delta^*$), there is a region in the $Da - \alpha Pe_m/z$ diagram of interphase kinetic control, where even though transport in the channel is free from limitation, the coating exhibits moderate diffusion effects (i.e. η takes values between the ones used as criteria for the internal regimes). This is found between the overall kinetic and intraphase control regime boundaries. Despite the fact that $Sh \simeq Sh_0$ still holds, now η cannot be described correctly by one of its asymptotes. Nevertheless, the approximation in Lopes et al. (2012b) for thin coatings (see Table 1) is also valid for nonlinear kinetics, by employing a kinetic normalization which is discussed in that reference. For example, for a second-order reaction, it was shown that the approximation has a relative error below 1.6% for coatings with $t_w \le a$. Although the boundary is not explicit in Da_{in}, it can be written in terms of the Graetz number, which appears in the developing contribution of $Sh_{0,dev}$ (Table 1). Thus, the boundary can still be obtained analytically (assigning values of Da_{in} between the predictions given by Eq.(T1) and (T9)):

$$Sh_0 = Da_{in}\,\eta\left(Da_{in}, \upsilon, \Delta, m\right)\frac{1-\theta}{\theta}. \qquad (31)$$

If $\eta \to 1$, Eq.(T3) is recovered. The area delimited by interphase kinetic control and interphase or overall mass transfer control corresponds to moderate limitations in the channel (θ between chosen criteria). The influence of the diffusion ratio can be depicted from Figure 9a: the region of interphase kinetic control is much narrower when Δ increases, while both boundaries of the mixed control area are dislocated towards lower values of Da_{in}.

Reactant inhibition effects

Reactant inhibition is translated by the magnitude of the dimensionless constant k' $(= k_{inh}\,\hat{c}_{in})$. Figure 9b shows the influence of increasing substrate inhibition on the regime boundaries in a $Da_{in} - k'$ plot. The following observations are relevant:

- The effect of k' is only visible when the *kinetic regime* is controlled by internal mass transfer. The "global reaction order" K_0 is a decreasing function of k' (see Eq.(T12) in

Table 2), increasing the limit value of Da_{in} up to the value where external mass transfer control is rate-limiting (kinetic independent). For the same parameters, inhibition moves the system from internal to external control.

- An inhibited kinetics requires higher values of Da_{in} to achieve *mass transfer control* if internal mass transfer is limiting when $k'=0$ (Eq.(T5) is an increasing function of k'). If Δ is high enough for relatively slow external mass transfer (compared to the internal one), then the boundary decreases (by one order-of-magnitude in Figure 9b, according to Eq.(T6)), until the minimum value of Da_{in} is dictated by external mass transfer. In mass transfer limited systems, inhibition increases the local Damköhler number by $\left(1+k'\right)^{2p/(m+1)}$. Thus, the effectiveness factor decreases for the same values of the parameters at the inlet, which explains the previous trends: a lower value of Da_{in} is required to attain a specified low value of η; and for the same $\theta\left(Da_{in}\,\eta\right)$, higher Da_{in} is needed to compensate internal limitations.
- The kinetic factor for *intraphase mass transfer control* (K_{∞} given by Eq.(T13) with $c_{surf}\to 1$) decreases with k'. Inhibition restricts the existence and area of this regime. On the other hand, it becomes more prevalent as $(m-p)$ increases, which represents the order of reaction in the limit of $k'\to\infty$.
- *Interphase control* would be only observed for $\Delta>17.3$ when $k'=0$ (first-order reaction), and this value becomes much higher for larger inhibition constants, since the global order of reaction for the cases in Figure 9b is below 1.

4.3 Catalyst layer design

Because in microchannel reactors the length scale for internal diffusion may be much smaller than the one in the channel, the *diffusion ratio* Δ (see Eq.(3)) may take higher values than those found for example, in diffusion through a stagnant film to a pellet in a fixed bed reactor. This is the relevant parameter to compare internal and external resistances (and not the ratios of diffusion timescales $D_{eff}\,a^2/(D\,t_w^2)$, or of diffusivities D_{eff}/D, or of thicknesses a/t_w, as it is often found in the literature). Even though mass transfer in the channel and coating are coupled, a $Da_{in}-\Delta$ diagram illustrates several features of the coating design (e.g. catalyst loading in Da_{in}, porous structure through D_{eff} and layer thickness t_w in Δ). This is plotted in Figure 10 for linear and nonlinear reactions. The following remarks can be made:

- The area under *kinetic control* is enlarged as the diffusion ratio is increased, but only up to the point (Eq.(T1)) where phenomena in the channel becomes controlling. Further

expansion is only obtained by increasing the flow parameter, reducing limitations in the channel.

- The opportunity to achieve *intraphase mass transfer control* decreases as the catalyst diffusion rate increases, but the upper boundary (related to the appearance of non-negligible limitations in the channel) is delayed by moving into the profile developing range.
- This inlet effect also makes *overall mass transfer control* harder to attain for low/moderate values of the diffusion ratio. For a first-order reaction, low values of the effectiveness factor in the catalyst are reached independently of the channel flow conditions. Thus, the lower limits for intraphase and catalyst controlled overall mass transfer control are given by the same expression (Eqs.(T6) and (T8)), though in different ranges of the diffusion ratio.
- For linear kinetics, *interphase control* is only observed at values of the diffusion ratio larger than those considered here: $\Delta > 17.3$ (value for a fully developed profile from Eq.(T10), $\theta = 0.9$).
- For *nonlinear kinetics*, the operating map is altered, especially under mass transfer control. This is notorious for a second-order reaction, and in general for any reaction with order above 1. Now both boundaries of the overall regime depend on the Graetz parameter. However, the interphase regime boundary is less sensitive (since for reasonable values of Δ, it depends on the fully developed value of Sherwood number) and corresponds to the minimum value of the Damköhler number for which strong limitation exists. The existence of this regime is restricted to large diffusion ratios if the profile is developing.

Figure 10a, valid for linear kinetics, also encloses some considerations related with *catalyst design*, namely loading, volume and existence of limitations to mass transfer. The washcoat loading may be included in the kinetic constant (or pre-exponential factor) as $k = \hat{k}\,\ell$ (Kočí et al., 2010), where ℓ is the concentration of active sites per volume of supported catalyst. The cost associated with the catalyst may be compared among different regimes in the $Da_{in} - \Delta$ map. Here, we will restrict ourselves to the comparison between operation under overall kinetic (K) and mass transfer (MT) control (the most extreme variation of design and operation). Considering the catalyst cost ($\text{cost} \sim V_{cat}\,\ell$, i.e. proportional to the mass of precious metal used) when operating at these two boundaries for $\Delta < \Delta^* \sim 1$, the same reaction temperature, effective diffusivity, metal dispersion, channel dimension a and fluid properties:

$$\frac{\text{cost}_\text{K}}{\text{cost}_\text{MT}} = \frac{3\,(1-\eta)}{Sh_\infty^2}\left(\frac{1-\theta}{\theta}\right)^2\left(\frac{D_{eff}}{D}\right)^2 \frac{a^2}{t_{w,\text{K}}\;t_{w,\text{MT}}}\,\frac{L_\text{K}}{L_\text{MT}}\,,$$

where $t_{w,\text{MT}} = V_{cat,\text{MT}}/S_{surf,\text{MT}}$, and assuming for example, $\eta = \theta = 0.9$. If the design is kept unaltered, then the cost of the catalyst in kinetic control is at least 3 orders of magnitude lower than in overall mass transfer control, decreasing as: $\text{cost}_\text{K}/\text{cost}_\text{MT} = \ell_\text{K}/\ell_\text{MT} \simeq 10^{-3}\,\Delta^2$. If the

microchannel is designed in order to attain the same fully developed conversion in both cases (same feed flowrate), then:

$$\frac{L_{\mathrm{K}}}{L_{\mathrm{MT}}} = \frac{Sh_{\infty}}{Da_{K}} \frac{\ln\left(1-X_{R}\right)}{\ln\left[\left(1-X_{R}\right)/w_{1,\infty}\right]} \simeq \frac{Sh_{\infty}}{3\left(1-\eta\right)\eta\,\Delta_{\mathrm{K}}} \sim \frac{10}{\Delta_{\mathrm{K}}} . \tag{32a}$$

Thus, the catalyst cost of a mass transfer limited system is more than 100 times higher, even though the microchannel can be at least 10 times shorter:

$$\frac{\mathrm{cost}_{\mathrm{K}}}{\mathrm{cost}_{\mathrm{MT}}} = \frac{1}{Sh_{\infty}} \left(\frac{1-\theta}{\theta}\right)^{2} \frac{1}{\eta} \Delta_{\mathrm{MT}} \sim \frac{\Delta_{\mathrm{MT}}}{100} . \tag{32b}$$

However, one also needs to take into account the costs due to increased equipment size and pressure drop. The ratio of these costs in kinetic and mass transfer control is assumed to be proportional to $L_{\mathrm{K}}/L_{\mathrm{MT}} \sim 10/\Delta_{\mathrm{K}}$. Including also this contribution into a "total cost" ($\mathrm{cost}_{\mathrm{total}}$), with the previous order-of-magnitude estimations:

$$\frac{\mathrm{cost}_{\mathrm{total,MT}}}{\mathrm{cost}_{\mathrm{total,K}}} = \frac{\Delta_{\mathrm{K}}}{10} + \left(\frac{10^{2}}{\Delta_{\mathrm{MT}}} - \frac{\Delta_{\mathrm{K}}}{10}\right) \frac{\mathrm{cost}_{\mathrm{K}}}{\mathrm{cost}_{\mathrm{total,K}}} . \tag{32c}$$

This implies that in order for the increased catalyst costs (due to higher loading in mass transfer control) to offset the higher capital and operating costs (due to larger microchannel size to attain the same conversion in kinetic control), the ratio between microchannel ($\mathrm{cost}_{\mathrm{K,ch}}$) and dilute catalyst ($\mathrm{cost}_{\mathrm{K}}$) costs in the kinetic boundary (where e.g. $\eta = 0.9$) should be higher than

$$\frac{\mathrm{cost}_{\mathrm{K,ch}}}{\mathrm{cost}_{\mathrm{K}}} > \frac{10}{\Delta_{\mathrm{MT}}} \frac{10^{2}-\Delta_{\mathrm{MT}}}{10-\Delta_{\mathrm{K}}} \sim \frac{10^{2}}{\Delta_{\mathrm{MT}}} . \tag{32d}$$

The estimated factors can be replaced by exact values, using the expressions above. Nevertheless, assuming a value for D_{eff}/D typical of Knudsen diffusion (e.g. 0.01), $a \sim 100\,\mu\mathrm{m}$ and feasible coating thickness $t_{w} > 1\,\mu\mathrm{m}$, full mass transfer control is economical if $\frac{\mathrm{cost}_{\mathrm{K,ch}}}{\mathrm{cost}_{\mathrm{K}}} > 100$.

Although this order-of-magnitude condition may seem unlikely, we note that it is possible that very low loading is required to attain $\eta = 0.9$ in kinetic control (active catalysts; high temperature operation), and that microfabrication and pressure drop costs are significant.

A similar analysis can be conducted when $\Delta > \Delta^{*} \sim 1$, i.e. when mass transfer control is defined by the catalyst and kinetic control by the channel, yielding the following considerations regarding the design of the catalyst layer:

$$\frac{\mathrm{cost}_{\mathrm{K}}}{\mathrm{cost}_{\mathrm{MT}}} = \frac{Sh_{\infty}}{\Delta_{\mathrm{MT}}} \upsilon_{\mathrm{MT}}\, \eta^{2} \sim \frac{1}{100\,\Delta_{\mathrm{MT}}} \tag{33a}$$

$$\frac{L_{\mathrm{K}}}{L_{\mathrm{MT}}} \simeq \frac{\left(1-\theta\right)}{\eta_{(\to 1)}\,\theta} \frac{Sh_{\infty}}{Sh_{0}} \sim 10 \tag{33b}$$

$$\frac{\text{cost}_{\text{total,MT}}}{\text{cost}_{\text{total,K}}} = 0.1 + \left(100\,\Delta_{\text{MT}} - 0.1\right)\frac{\text{cost}_{\text{K}}}{\text{cost}_{\text{total,K}}}. \tag{33c}$$

Operating in overall mass transfer control is beneficial if

$$\frac{\text{cost}_{\text{K,ch}}}{\text{cost}_{\text{K}}} > \frac{100\,\Delta_{\text{MT}} - 1}{0.9} \sim 100\,\Delta_{\text{MT}}. \tag{33d}$$

The excess of microchannel costs (regarding equipment and pressure drop in kinetic control) required for overall mass transfer control to be beneficial, is minimum when $\Delta \sim 1$, i.e. in the intermediate regime regarding internal/external diffusion. Considering moderate, instead of severe, mass transfer limitations (perhaps in an interphase controlled regime, if attainable) should yield less strict conditions on $\text{cost}_{\text{K,ch}}/\text{cost}_{\text{K}}$ for the total cost to be reduced, when compared to Eqs.(32d) and (33d) (the most unfavorable cases). Thus, it is very likely that *moderate external (and when unavoidable, also internal) limitations make the system more cost effective for feasible ratios of the expenditures associated with the channel and the catalyst under kinetic control.*

5 DESIGN EVALUATION

5.1 Design in the presence of a constraint on conversion

When a given level of conversion is fixed, Damköhler and Graetz numbers are related (translated by an iso-conversion curve in a $Da_{in} - \alpha Pe_m/z$ plot, Figure 11). However, each point in this curve is characterized by different requirements due to pressure drop and energetic input.

The dimensionless pressure drop ΔP (Eq.(6)) can be written explicitly in terms of the specified value of conversion by making use of simplified results (Lopes et al., 2011b). Figure 5a shows that appreciable reactant conversion will only be found when operation occurs close to full profile development. Consequently, higher dimensionless pressure drops must be faced (i.e. for the same fluid velocity, the microchannel needs to be longer). Under these conditions, the $\Delta P\left(Da, X_R\right)$ dependence for linear kinetics is given explicitly by

$$\Delta P \simeq \frac{C_D\,Sc}{2}\ln\left[\frac{w_1\left(Da\right)}{1 - X_R}\right]\left(\frac{1}{Da} + \frac{1}{Sh_{\infty,\,fd}}\right). \tag{34}$$

Calculation of w_1 and $Sh_{\infty,\,fd}$ were detailed in Lopes et al. (2011b). Note that the product $C_D = f_D\,Re$ is known for several geometries. Eq.(34) is plotted in Figure 11 for specified values of X_R, in terms of the inlet Damköhler number (note that $Da = \eta\,Da_{in}$, but the effectiveness factor does not change with the axial position and can be easily calculated with the approximation in Lopes et al. (2012b)). The minimum value of conversion predicted from this

model with controlling mass transfer and with error ε_{fd} is calculated as a function of Da_{in} by Eq.(15). For laminar flow inside a circular channel, if $X_R > 0.67$, the relative error stays below 0.1%.

The asymptote of ΔP close to the regime delimitated by the boundaries intersecting at $\mathbf{V_1}$ **(high conversion)** is

$$\Delta P = \Delta P_\infty + \left(Sh_{\infty,fd}\ \Delta P_\infty + \frac{C_D\ Sc}{2\ Sh_{\infty,fd}} \right) \frac{1}{Da} + O\left(Da^{-2}\right) \qquad \text{for } Da \to \infty . \tag{35}$$

The minimum dimensionless pressure drop required to attain X_R, occurs under total mass transfer control, and is given by:

$$\Delta P_\infty = \frac{C_D\ Sc}{2\ Sh_{\infty,fd}} \ln\left(\frac{w_{1,\infty}}{1 - X_R} \right). \tag{36}$$

For the region converging in $\mathbf{V_5}$ **(homogeneous microreactor)**:

$$\Delta P = \frac{C_D\ Sc}{2\ Da} \ln\left(\frac{1}{1 - X_R} \right) + O\left(Da\right) \qquad \text{for } Da \to 0 . \tag{37}$$

The dimensionless pressure drop (channel length) given in (34) is minimized for a given X_R, when Da_{in} (or Da) is increased. On the other hand, the maximum conversion obtained from a developing profile (associated with lower values of ΔP) is quite low (see Eq.(22)). Thus, to meet a strict target, working on a high- ΔP and/or Da regime is required. *Possible improvement keeping the same X_R, implies moving to the intermediate regime concerning mass transfer control, but not with respect to the profile development.* The results of Lopes et al. (2011b) are of interest when changes in the intensity of the reaction rate (keeping a fully developed profile) are considered.

5.1.1 Operating limit on Da

The minimum pressure drop ΔP_∞ guideline is not a clear recommendation since as we showed in section 4, the delimitation of the mass transfer controlled regime may depend on several parameters/criteria. Moreover, other considerations (e.g. external heating demands or catalyst and equipment preservation) only allow this asymptote ($Da \to \infty$) to be fulfilled within a certain non-negligible margin. Thus, it is reasonable to assume that a maximum allowable reaction rate exists (translated into a specified value of $Da_{\max}$, with maximum temperature and/or catalyst loading). The excess dimensionless pressure drop ($\Delta P_{exc} = \Delta P - \Delta P_\infty$) to be accommodated by not operating at $Da \to \infty$ is taken from (35) and has the following dependence:

$$\Delta P_{exc} \simeq \frac{Sh_{\infty,fd}\ \Delta P_\infty}{Da_{\max}} . \tag{38}$$

It is assumed that this maximum value of Da is still close to mass transfer control. Near complete conversion, the additional term to the excess pressure drop expressing the $w_1(Da)$ dependence is negligible in Eq.(35). If a severe constraint in the value of Da exists (moderate to low values of $Da_{\max}$), then Eq.(34) should be used to compute ΔP_{exc}.

The influence of internal diffusional limitations ($\eta << 1$) is to increase the dimensionless pressure drop required to attain a conversion X_R for the same value of Da_{in}. In this analysis, it is likely that appreciable diffusional effects in the catalyst appear in overall mass transfer control (intraphase control is more commonly found under developing profile conditions if the diffusion ratio Δ is not too small; interphase control is only possible for $\Delta > Sh_\infty \upsilon/(1-\theta)$, with θ close to 1). In this case, Eq.(38) becomes

$$\Delta P_{exc} = \frac{Sh_{\infty,fd}\ \Delta P_\infty}{\sqrt{Da_{in,\max}}} \sqrt{\frac{\upsilon}{\Delta}}\ . \tag{39}$$

Eqs. (38) and (39) are quantitative design rules, which precise the penalties in pressure drop for not meeting the $Da \to \infty$ condition exactly. These can be derived by taking into consideration the knowledge of the asymptotic behavior near mass transfer control, given in Eq.(35).

5.1.2 Tolerable ΔP increase

A reduction in Da_{in} is achieved if a pressure drop above ΔP_∞ can be tolerated. If the admissible value of $\Delta P = \Delta P_{\max} + \Delta P_\infty$ is high enough, operation will fall out of mass transfer control (for $\Delta P_{\max} > \Delta P_1/\theta - \Delta P_\infty$) and a conservative estimate for the minimum value of Da is

$$Da_{\min} = \frac{Sh_{\infty,fd}\ \Delta P_1}{\Delta P_{\max} + \Delta P_\infty - \Delta P_1}\ , \tag{40a}$$

where $\Delta P_1 = \frac{C_D\ Sc}{2\ Sh_{\infty,fd}} \ln\left(\frac{1}{1-X_R}\right)$. (40b)

For example, if $X_R = 0.95$ in a gas-phase laminar flow, a minimum increase of 19% is required on top of ΔP_∞ to fall out of mass transfer control ($\theta < 0.9$) in a circular microchannel and this occurs when $Da_{\min} < 16.5$. For small increases in pressure drop (remaining under mass transfer control), Eq.(38) can be used with $\Delta P_{exc} \equiv \Delta P_{\max}$ and $Da_{\max} \equiv Da_{\min}$. In this case, it is likely that diffusional limitations are also present in the catalyst (thus, Eq.(39) applies): $Da_{in,\min} \sim (\Delta P_\infty)^2 \big/ \left[\Delta\, (\Delta P_{\max})^2\right]$.

The energetic gain compared to the maximum operating value $Da_{\max}$ is

$$\frac{\Delta Da}{Da_{\max}} = \frac{Da_{\max} - Da_{\min}}{Da_{\max}} = 1 - \frac{\Delta P_1}{\Delta P_\infty}\ \frac{\Delta P_{exc}}{\Delta P_{\max} + \Delta P_\infty - \Delta P_1}\ .$$

For high X_R, $\Delta P_\infty \simeq \Delta P_1$ and therefore

$$\frac{\Delta Da}{Da_{\max}} = 1 - \frac{\Delta P_{exc}}{\Delta P_{\max}}.$$

In this problem, $\Delta P_{\max}$, $Da_{\max}$ and X_R are specified. If $\Delta P_{\max} \to \infty$ there is no pressure drop limitation, whereas if $Da_{\max} \to \infty$, operation at high temperature or with highly active catalysts is feasible. The effect of internal diffusional limitations is to increase $Da_{in,\min}$ (to its square value as seen above), thus reducing significantly the energetic gain.

Several variables may influence Da. In particular, the decrease in operating temperature ($\Delta T = T_{\max} - T$) from its maximum value ($T_{\max}$) is

$$\frac{\Delta T}{T_{\max}} = \frac{2\ln\left(\Delta P_{\max}/\Delta P_{exc}\right)}{2\ln\left(\Delta P_{\max}/\Delta P_{exc}\right) + \gamma_{\max}} \qquad (T_{\min} \text{ is in overall mass transfer control}) \qquad (41a)$$

$$\frac{\Delta T}{T_{\max}} = \frac{2\ln\left(\dfrac{\Delta P_{\max}}{\Delta P_{exc}}\sqrt{\dfrac{Da_0\,\upsilon}{\Delta}}\right) - \gamma_{\max}}{2\ln\left(\dfrac{\Delta P_{\max}}{\Delta P_{exc}}\sqrt{\dfrac{Da_0\,\upsilon}{\Delta}}\right) + \gamma_{\max}} \qquad (T_{\min} \text{ is in internal kinetic control}) \qquad (41b)$$

where the Arrhenius parameter at $T_{\max}$ is $\gamma_{\max} = E/(R_G T_{\max})$, $Da_0 = a\,k_{0,surf}/D$ and ΔP_{exc} is given by Eq.(38). A similar analysis is possible for the effect of the washcoat loading. Eqs.(41) are the basis to compare the pressure drop that can be tolerated ($\Delta P_{\max}$), with the energetic requirements (ΔT) to achieve a certain inlet reaction rate. *This will move the optimum design from the mass transfer controlled and fully developed profile to the intermediate (reaction-transport) region.*

5.2 Trade-offs in microreactor performance

Designs of an isothermal microreactor in the previously well identified regimes may be evaluated under the light of the following criteria: reactant conversion (X_R), flow efficiency (defined by Kolodziej et al. (2007) as $1/\Delta P$) and reactor effectiveness ($\bar{\eta}$), given by

$$\bar{\eta} = \frac{\iiint \hat{R}(\hat{c})\,dV_{cat}}{\hat{R}(\hat{c}_{in})\,V_{cat}} = \frac{\alpha\,Pe_{m,\max}/z}{\sigma_C\,Da_{in}}\,X_R, \qquad (42)$$

i.e. the average reaction rate in the reactor compared with the one that would be observed at inlet conditions. For a first-order reaction, it is related with η and the average of the surface reaction rate.

It is hardly acceptable that simultaneous consideration of these factors yields an optimum design or operation in extremities of the $Da_{in} - \alpha\,Pe_m/z$ diagram. Yet, this is what is predicted

by most criteria in the literature. Each vertex in Figure 6, outside of the intermediate region, privileges one of the design goals. Figure 12 clarifies the trade-offs that the intermediate regime carries. As seen in section 5.1, the pressure drop – conversion binomial will always favor mass transfer controlled regime for attaining high conversions (vertex $\mathbf{V_1}$). In the limit, this would imply infinite operating temperatures and catalyst activity, or infinitely long channels, etc. The former trend is associated with a number of problems (intense external heating, catalyst deactivation, parasite reactions, activation of homogeneous reactions, etc.), while the latter direction has significant pressure drop issues. Decrease of conversion (in the same order of magnitude) can proceed towards high effectiveness (lower energy requirement for reaction in $\mathbf{V_5}$, but larger reactor) or by decreasing the channel length (hence the pressure drop) when directed to $\mathbf{V_2}$ (with roughly the same low value for effectiveness). High effectiveness and flow efficiency are observed at $\mathbf{V_4}$, but conversion decreases two orders-of-magnitude. The segment $\mathbf{V_4}$ **-** $\mathbf{V_5}$ is characterized by low transport resistance (high $\bar{\eta}$), while conversion and efficiency vary with opposite trends. The extent of these limitations increases sharply (by 3 orders of magnitude) when moving to other regions in the diagram. The $\mathbf{V_2}$ **–** $\mathbf{V_4}$ side has high flow efficiency, since profile is developing. The conversion plot is nearly symmetric with respect to the $\mathbf{V_1}$ **–** $\mathbf{V_4}$ axis, as can also be observed in Figure 5a.

Table 3 shows the dependence of performance factors on the criteria (θ, η, ε_{fd} and e_{dev}) that define the boundaries in Figure 6 ($\Delta < \Delta^*$). Numerical values are based on laminar flow inside a circular microchannel, but general expressions can be easily obtained from the results in sections 3 and 4. If an overall performance metric includes the aforementioned criteria ($X_R, 1/\Delta P$ and $\bar{\eta}$), then the trends in Table 3 clarify the direction towards the optimal design.

6 CONCLUSIONS

This work presents an analysis of the mass transfer – reaction phenomena in coated microreactors and an evaluation of their performance under different conditions. The modeling approach presented here contributes to *map and describe the behavior of systems characterized by different degrees of transport resistance and reaction intensity*. Namely:

1. The dependence of the applicability ranges of mass transfer models on the wall reaction rate is given here for the first time in an explicit manner (also as a function of the level of agreement specified and channel shape and flow factors). This dependence was found to be quite strong and to present an inverse trend from that exhibited by the entrance length derived from the Sherwood number profile, from Neumann to Dirichlet boundary conditions (as the Damköhler number Da increases).
2. The most peculiar behavior of the relative errors associated with limiting descriptions of the concentration profile development appeared for intermediate and low reaction rates (values

of $Da \lesssim 1$). In particular, the adequacy of the fully developed regime increases almost up to the inlet, as the reactant sink at the wall becomes weaker. This is contrary to what is perceived from classical results.

3. For $Da \gtrsim 1$, the dimensionless fully developed channel length varies less significantly with Da. These conclusions were obtained by considering the profile structure predicted by a more complete solution for this problem (which can be extended to other Graetz and Lévêque problems). This improved expression combines and weighs analytically developing and developed contributions in the final result.
4. The superposition of the ranges for convection-diffusion and reaction-transport controlling regimes yields 4 distinct regions in a reaction – flow (Da-Graetz) map: high conversion, hot inlet, homogeneous, and low conversion. The maximum or minimum conversion that can be attained in each area can be easily calculated by explicit functions of the relative errors that can be tolerated. These boundaries limit an intermediate region.
5. Diagnosis of mass transfer limitations in planes of the multi-parameter space characterizing the channel-coating system behavior was accomplished in conditions of nonlinear and inhibited kinetics. The order of reaction m (especially whether it is higher or lower than 1) was found to have a profound effect on the regimes that were observed. For example if $m < 1$, interphase resistance can be suppressed and overall mass transfer control is not determined by the catalyst. Increasing inhibition in the system, leads to a reduction of the intraphase resistance regime and leaves the regimes to be defined by the channel features. The analytical methodology used is general, and yields explicit parametric dependence. Furthermore, it is able to encompass a wide range of complex phenomena (developing flows, arbitrary geometries, etc.) which allows the description of the behavior of many systems.
6. We presented, for the first time, the proper mapping of the relative internal-external diffusional limitations (governed by the 'diffusion ratio' Δ) against the (linear or nonlinear) reaction rate. This new representation is very relevant in coated microchannels, as they open the $\Delta \gtrsim 1$ space. This was interpreted from a catalyst design point of view. For nonlinear kinetics, the effects of the reactant distribution across the fluid-solid interface identified in Lopes et al. (2012c) were also observed (i.e. prevalence of the interphase regime for kinetics with $m > 1$ in the high conversion region; requirement of high reaction rates to achieve low effectiveness factor in very externally mass transfer limited systems, etc). Moreover, a region of interphase kinetic control (where channel is kinetically controlled, while the coating exhibits moderate diffusional limitations) was identified, leaving the remaining area (with mixed control) much better delimitated in this comprehensive picture.

The results presented here also allow us to understand *the role of the intermediate convection-diffusion-reaction region*:

7. As Da decreases, the transition region between entrance-length and profile full development is replaced by an overlapping region. This means that the fast transport mechanisms in the intermediate region balance as $Da \to 0$. On the other hand, under high mass transfer resistance, the transition region may occupy several orders of magnitude of the dimensionless length. To describe this situation, the solution given in Lopes et al. (2012a) is required, as none of the simplest models is accurate enough.
8. The intermediate region is surrounded by different areas of kinetic and mass transfer control. In general, moderate levels of mass transfer limitation are present at least in one of the domains. For example, in Figure 9a, two more areas inside the intermediate region can be identified: gradientless transport in the channel towards a coating with some limitations, but not yet in the diffusional regime (between the kinetic control and intraphase regime boundaries); and a mixed control regime with moderate resistance in the channel.
9. It was shown with simple costing arguments, that operating in the presence of moderate mass transfer resistance (thus, out of overall kinetic control) may be beneficial. The most unfavorable case of overall mass transfer control (in both the catalyst and channel) was analyzed, and the conditions for cost reduction were derived.
10. A minimum pressure drop design for appreciable conversion requires operation close to full development and mass transfer control. This objective is not met when moving to the intermediate convection-diffusion area, and is very sensitive to the proper delimitation of the high conversion region (thus, order-of-magnitude estimates based on intersecting asymptotes are not suitable). However, consideration of energy input (maximum reaction rate) together with higher allowable pressure drop (higher channel length) suggests that less unbalanced relative rates between reaction and transport may be optimal.
11. The distribution of the 3 performance factors (effectiveness, flow efficiency and conversion) among the previously identified regimes shows the different trade-offs that are present and the penalties that one needs to face when privileging a single objective. Ultimately, the importance of each factor depends on the particular application, but our analysis is kept general with the characterization and delimitation of the different design/operation *loci* in the parametric space. However, it is likely that in many cases there is not a single dominant factor. In this case, higher benefits can be taken from locating the design in the intermediate region.

NOTATION

a	channel transverse characteristic length (radius of a circular channel, slit half width spacing), m
A, B	numerical constants
c	dimensionless concentration of reactant in the channel ($c = \hat{c} / \hat{c}_{in}$)
$\langle c \rangle$	dimensionless mixing-cup concentration of reactant in the channel (averaged with velocity profile over the channel's cross-section)

$\hat{c}_{in}$	inlet channel concentration, $\mathrm{mol}/\mathrm{m}_{\mathrm{f}}^3$
c_{surf}	dimensionless concentration of reactant at the channel-coating interface ($c_{surf} = \hat{c}_{surf} / \hat{c}_{in}$)
C_D	Darcy's friction factor coefficient, $C_D = f_D \, Re$
D	bulk channel diffusivity, m^2/s
D_{eff}	effective diffusivity in the catalytic coating, m^2/s
Da	Second Damköhler number (Damköhler, 1937), including internal effects, $a \, \eta \, \hat{R}_{surf} / (\hat{c}_{surf} D)$
Da_{in}	Second Damköhler number referred to inlet conditions, $a \, \hat{R}_{surf}(\hat{c}_{in}) / (\hat{c}_{in} D)$
e_{dev}	relative error of developing profile asymptote relative to inlet concentration
f_D	Darcy's friction factor
${}_2F_1$	regularized hypergeometric function
k	kinetic constant for reaction with order m, $\mathrm{mol}^{1-m}(\mathrm{m}^3)^{m-1}\mathrm{s}^{-1}$
$\hat{k}$	kinetic constant for unit loading, $\mathrm{mol}^{1-m}(\mathrm{m}^3)^{m}\mathrm{s}^{-1}$ (mol precious metal)$^{-1}$
k'	dimensionless kinetic parameter
k_{inh}	inhibition constant, $\mathrm{m}^3/\mathrm{mol}$
k_m	mass transfer coefficient, $\mathrm{m/s}$
k_0	pre-exponential factor, $\mathrm{mol}^{1-m}(\mathrm{m}^3)^{m-1}\mathrm{s}^{-1}$
K_0	kinetic normalization factor in the catalyst's chemical regime
K_∞	kinetic normalization factor in the catalyst's diffusional regime
L	length of the channel, m
ℓ	catalyst loading concentration, mol precious metal/m_{cat}^3
m	order of reaction
M	numerical coefficient
N	numerical coefficient
p	exponent in reaction kinetic law
Pe_m	mass Peclet number, $a\langle u \rangle / D$
ΔP	dimensionless pressure drop, given in Eq.(6)
Q_V	flowrate, $\mathrm{m}_{\mathrm{f}}^3/\mathrm{s}$
R	dimensionless reaction rate, normalized by rate at inlet conditions
$\hat{R}_{surf}$	dimensional reaction rate per wall surface area, $\mathrm{mol}/(\mathrm{m}_{\mathrm{wall}}^2\mathrm{s})$
$\hat{R}_{surf,obs}$	dimensional observed reaction rate, per surface area $\mathrm{mol}/(\mathrm{m}_{\mathrm{wall}}^2\mathrm{s})$
$\hat{R}_V$	dimensional reaction rate per washcoat volume, $\mathrm{mol}/(\mathrm{m}_{\mathrm{cat}}^3\mathrm{s})$
Re	Reynolds number, $= a \, \rho \langle u \rangle / (2 \, \mu)$
S	channel's shape factor
S_{surf}	area of the channel-coating interface, m^2
Sc	Schmidt number, $= \mu / (\rho D)$
Sh	Sherwood number, $= a \, k_m / D$
Sh_0	Sherwood number for Neumann (uniform flux) wall boundary condition
Sh_∞	Sherwood number for Dirichlet (uniform concentration) wall boundary condition
t_w	washcoat characteristic thickness, m
u	fluid velocity in the channel, $\mathrm{m/s}$
$\langle u \rangle$	average fluid velocity in the channel, $\mathrm{m/s}$
V_{cat}	washcoat volume, m_{cat}^3
X_R	reactant conversion
z	dimensionless axial coordinate (normalized by channel length L), $\hat{z} = z \, L$

Greek letters

α aspect ratio of the channel (a / L)
$\alpha Pe_m / z$ Graetz number evaluated with average velocity (product of transverse Peclet number and aspect ratio), Eq.(1)
$\alpha Pe_{m,max} / z$ Graetz number evaluated with maximum velocity
Δ diffusion ratio, given in Eq.(3)
ε ratio of the characteristic distances for diffusion in the coating and in the channel
ε_{fd} relative deviation between actual conversion and fully developed prediction
μ dynamic viscosity, Pa.s
η catalytic coating effectiveness factor (referred to local fluid-solid interface conditions), Eq.(26)
$\bar{\eta}$ reactor effectiveness (referred to inlet conditions), Eq.(42)
ρ fluid density, kg/m^3
σ_C channel's shape parameter, Eq.(5)
θ degree of mass transfer control, Eq.(25)
ν kinematic viscosity ($= \mu / \rho$), m^2/s
Λ geometry factor for catalyst coating in kinetic regime
υ catalyst volume to surface ratio, divided by characteristic dimension for diffusion, Eq.(4)

Superscripts
^ dimensional quantities

Subscripts
D Darcy
dev developing conditions
fd fully developed conditions
in referred to inlet conditions
surf referred to surface conditions, per channel-washcoat surface area
V per volume of washcoat
0 conditions of uniform wall flux
∞ condition of wall concentration annulment

ACKNOWLEDGEMENTS

J. P. Lopes gratefully acknowledges financial support from FCT – Fundação para a Ciência e a Tecnologia (SFRH/BPD/81532/2011).

REFERENCES

Al-Rawashdeh, M.m., Nijhuis, X., Rebrov, E.V., Hessel, V., Schouten, J.C., 2012. Design methodology for barrier-based two phase flow distributor. AIChE Journal 58, 3482-3493.

Alfieri, F., Tiwari, M.K., Zinovik, I., Brunschwiler, T., Michel, B., Poulikakos, D., 2012. On the significance of developing boundary layers in integrated water cooled 3D chip stacks. International Journal of Heat and Mass Transfer 55, 5222-5232.

Berger, R.J., Kapteijn, F., 2007a. Coated-wall reactor modeling-criteria for neglecting radial concentration gradients. 1. Empty reactor tubes. Industrial and Engineering Chemistry Research 46, 3863-3870.

Berger, R.J., Kapteijn, F., 2007b. Coated-wall reactor modeling-criteria for neglecting radial concentration gradients. 2. Reactor tubes filled with inert particles. Industrial and Engineering Chemistry Research 46, 3871-3876.

Cao, C., Palo, D.R., Tonkovich, A.L.Y., Wang, Y., 2007. Catalyst screening and kinetic studies using microchannel reactors. Catalysis Today 125, 29-33.

Damköhler, G., 1937. Einfluss von Diffusion, Strömung, und Wärmetransport auf die Ausbeute in Chemisch-Technischen Reaktionen. Chem.-Eng.-Tech 3, 359-485.

Fu, H., Dencic, I., Tibhe, J., Sanchez Pedraza, C.A., Wang, Q., Noel, T., Meuldijk, J., de Croon, M., Hessel, V., Weizenmann, N., Oeser, T., Kinkeade, T., Hyatt, D., Van Roy, S., Dejonghe, W., Diels, L., 2012. Threonine aldolase immobilization on different supports for engineering of productive, cost-efficient enzymatic microreactors. Chemical Engineering Journal 207–208, 564-576.

Fukuda, T., Maki, T., Mae, K., 2012. Design of a Plate-Type Catalytic Microreactor with CO 2 Permeation Membrane for Water-Gas Shift Reaction. Chemical Engineering and Technology 35, 1205-1213.

Gervais, T., Jensen, K.F., 2006. Mass transport and surface reactions in microfluidic systems. Chemical Engineering Science 61, 1102-1121.

Gonzo, E.E., Gottifredi, J.C., 2011. Heat and mass transfer limitations in monolith reactor simulation with non uniform washcoat thickness. Latin American Applied Research 40, 15-21.

Groppi, G., Ibashi, W., Tronconi, E., Forzatti, P., 2001. Structured reactors for kinetic measurements under severe conditions in catalytic combustion over palladium supported systems. Catalysis Today 69, 399-408.

Hernández Carucci, J.R., Eränen, K., Murzin, D.Y., Salmi, T.O., 2009. Experimental and modelling aspects in microstructured reactors applied to environmental catalysis. Catalysis Today 147, S149-S155.

Hessel, V., Cortese, B., de Croon, M.H.J.M., 2011. Novel process windows - Concept, proposition and evaluation methodology, and intensified superheated processing. Chemical Engineering Science 66, 1426-1448.

Joshi, S.Y., Harold, M.P., Balakotaiah, V., 2010. Overall mass transfer coefficients and controlling regimes in catalytic monoliths. Chemical Engineering Science 65, 1729-1747.

nsan, Z.I., 2009. Steady-state and dynamic modeling of indirect partial oxidation of methane in a wall-coated microchannel. Catalysis Today 139, 312-321.

Kays, W.M., Crawford, M.E., 1980. Convective Heat and Mass Transfer, Second Edition ed. McGraw-Hill, New York.

Kočí, P., Novák, V., Štěpánek, F., Marek, M., Kubíček, M., 2010. Multi-scale modelling of reaction and transport in porous catalysts. Chemical Engineering Science 65, 412-419.

Kolb, G., Zapf, R., Hessel, V., Löwe, H., 2004. Propane steam reforming in micro-channels—results from catalyst screening and optimisation. Applied Catalysis A: General 277, 155-166.

Kolodziej, A., Lojewska, J., 2007. Short-channel structured reactor for catalytic combustion: Design and evaluation. Chemical Engineering and Processing: Process Intensification 46, 637-648.

Lopes, J.P., Cardoso, S.S., Rodrigues, A.E., 2011a. Criteria for kinetic and mass transfer control in a microchannel reactor with an isothermal first-order wall reaction. Chemical Engineering Journal 176-177, 3-13.

Lopes, J.P., Cardoso, S.S.S., Rodrigues, A.E., 2012a. Bridging the gap between Graetz's and lévêque's analyses for mass/heat transfer in a channel with uniform concentration or flux at the wall. AIChE Journal 58, 1880-1892.

Lopes, J.P., Cardoso, S.S.S., Rodrigues, A.E., 2012b. Effectiveness factor for thin catalytic coatings: Improved analytical approximation using perturbation techniques. Chemical Engineering Science 71, 46-55.

Lopes, J.P., Cardoso, S.S.S., Rodrigues, A.E., 2012c. Interplay between channel and catalyst operating regimes in wall-coated microreactors. Chemical Engineering Journal 10.1016/j.cej.2012.11.056.

Lopes, J.P., Rodrigues, A.E., Cardoso, S.S., 2011b. Approximate calculation of conversion with kinetic normalization for finite reaction rates in wall-coated microchannels. AIChE Journal 57, 2870-2887.

Mariani, N.J., Keegan, S.D., Martínez, O.M., Barreto, G.F., 2008. On the evaluation of effective reaction rates on commercial catalyst by means of a one-dimensional model. Catalysis Today 133-135, 770-774.

Mocciaro, C., Mariani, N.J., Martínez, O.M., Barreto, G.F., 2011. A three-parameter one-dimensional model to predict the effectiveness factor for an arbitrary pellet shape. Industrial and Engineering Chemistry Research 50, 2746-2754.

Norton, D.G., Wetzel, E.D., Vlachos, D.G., 2005. Thermal Management in Catalytic Microreactors. Industrial & Engineering Chemistry Research 45, 76-84.

Papadias, D., Edsberg, L., Björnbom, P., 2000. Simplified method for effectiveness factor calculations in irregular geometries of washcoats. Chemical Engineering Science 55, 1447-1459.

Rebrov, E.V., Duinkerke, S.A., de Croon, M.H.J.M., Schouten, J.C., 2003. Optimization of heat transfer characteristics, flow distribution, and reaction processing for a microstructured reactor/heat-exchanger for optimal performance in platinum catalyzed ammonia oxidation. Chemical Engineering Journal 93, 201-216.

Redlingshöfer, H., Kröcher, O., Böck, W., Huthmacher, K., Emig, G., 2002. Catalytic wall reactor as a tool for isothermal investigations in the heterogeneously catalyzed oxidation of propene to acrolein. Industrial and Engineering Chemistry Research 41, 1445-1453.

Renken, A., Kiwi-Minsker, L., 2008. Chemical Reactions in Continuous–flow Microstructured Reactors, in: Kockmann, N. (Ed.), Micro Process Engineering: Fundamentals, Devices, Fabrication, and Applications. Wiley-VCH Verlag GmbH, Weinheim, Germany, pp. 173-201.

Rosa, P., Karayiannis, T.G., Collins, M.W., 2009. Single-phase heat transfer in microchannels: The importance of scaling effects. Applied Thermal Engineering 29, 3447-3468.

Saber, M., Commenge, J.M., Falk, L., 2010. Microreactor numbering-up in multi-scale networks for industrial-scale applications: Impact of flow maldistribution on the reactor performances. Chemical Engineering Science 65, 372-379.

Salmi, T., Hernández Carucci, J., Roche, M., Eränen, K., Wärnå, J., Murzin, D., 2013. Microreactors as tools in kinetic investigations: Ethylene oxide formation on silver catalyst. Chemical Engineering Science 87, 306-314.

Shah, R.K., London, A.L., 1978. Laminar flow forced convection in ducts. Academic Press, New York.

Tadepalli, S., Halder, R., Lawal, A., 2007. Catalytic hydrogenation of o-nitroanisole in a microreactor: Reactor performance and kinetic studies. Chemical Engineering Science 62, 2663-2678.

Wijngaarden, R.J., Kronberg, A., Westerterp, K.R., 1998. Industrial catalysis: optimizing catalysts and processes Wiley-VCH, Weinheim.

FIGURE CAPTIONS

Figure 1: Interaction between transport and reaction mechanisms in a wall coated microreactor. Parameters are presented in section 2. The vertices denote regimes where dominant (fast) mechanisms prevail.

Figure 2: Schematic representation of a coated microchannel and main design variables.

Figure 3: Fully developed boundary in a $Da - z/\alpha Pe_m$ map for laminar flow (a) between parallel plates and (b) inside a circular channel. The analytical prediction (full lines) given by Eq. (19) improves as ε_{fd} decreases and gives a very reasonable description even at intermediate values of the Damlöhler number. The deviation calculated through the numerical evaluation of Eq.(7) with a large number of terms is represented by points.

Figure 4: Developing profile boundary in a $Da - z/\alpha Pe_m$ plot for laminar flow (a) between parallel plates and (b) inside a circular channel. Analytical predictions at high and low Damköhler number are given by Eqs.(21) and (24).

Figure 5: Applicability range of mass transfer models. (*a*) $Da - \alpha Pe_m / z$ map. Prediction of reactant conversion X_R in fully developed conditions (thin full line) or at the entrance length (thin dashed line). Overlapping region (where both models agree) and transition region (where both models fail) are also shown (boundaries given by thick lines). (*b*) X_R as a function of $z/\alpha Pe_m$ for several values of Da (change between overlapping and transition regions occurs at $Da \simeq 0.95$). Results for laminar flow inside a circular channel.

Figure 6: Damköhler – Graetz plot for a first-order reaction occurring in an annular coating in a circular channel with laminar flow ($\upsilon = 1.05$). Regime boundaries are plotted for $\Delta = 0.1$ and $\Delta = 1$ (internal control: $\eta \le 0.1$; external control: $\theta \ge 0.9$; no internal limitation: $\eta \ge 0.9$; no external limitation: $\theta \le 0.1$; developed profile: $\varepsilon_{fd} \le 1\%$; developing profile: $e_{dev} \le 1\%$). Vertices (V) delimiting the intermediate regime (shaded region) are discussed in the text.

Figure 7: Adequacy of the mass transfer control regime boundary derived with Dirichlet and Neumann boundary conditions. Analytical calculations (lines) using Eq.(T5) are compared with the numerical simulation from a 2-dimensional model (points) including axial diffusion effects for $\theta = 0.90$, $Pe_m = 100$, $\upsilon = 1.01$, $Sc = \infty$ and $\Delta = 0.1$ in a circular channel.

Figure 8: Effect of simultaneous hydrodynamic developing flow in regime mapping. Lines obtained analytically from Eqs.(T2) and (T5) for several values of Schmidt number (Sc). The data set (1) should be read on the left side vertical axis ($\Delta = 0.1$ and $\theta = 0.9$); while data set (2) can be read in the right side vertical axis ($\Delta = 0.2$ and $\eta = 0.9$).

Figure 9: Reaction nonlinearities in regimes with kinetic (KC) and mass transfer control (MTC). (a) $Da_{in} - \alpha\, Pe_m / z$ plot for $m = 2$, $k' = 0$ and $\upsilon = 1.05$. (b) Influence of the reactant inhibition constant k' on regime boundaries: Overall kinetic control (KC) for fully developed profile; Overall mass transfer control (MTC) for $z/\alpha\, Pe_m = 0.1$; and Intraphase mass transfer control (MTC) for $z/\alpha\, Pe_{m,\max} = 10^{-4}$.

Figure 10: $Da_{in} - \Delta$ operating map for a circular channel with laminar flow coated with an annular catalyst layer ($\varepsilon = 0.1$). (a) First-order reaction ($m = 1$). (b) Second-order reaction ($m = 2$). External and internal mass transfer control observed for $\theta = 0.9$ and $\eta = 0.1$, respectively. Negligible resistances for $\theta = 0.1$ and $\eta = 0.9$. Full lines associated with conditions in channel are plotted for values of the Graetz parameter. The area for overall kinetic control (Ov. KC) is depicted as well as the ones for mass transfer control: overall (Ov. MTC), internal (Intraph. MTC) and external (Interph. MTC). Pictures in (a) illustrate schematically the catalyst volume (not to scale) and loading in 4 areas of the diagram.

Figure 11: Design in the $Da_{in} - \Delta P$ diagram for specified conversion X_R. For a given X_R, the minimum pressure drop ΔP_∞ given by Eq.(36), increases by ΔP_{exc} if a maximum reaction rate exists ($Da_{in,\max}$), as suggested by Eq.(39). If further increase is acceptable (by $\Delta P_{\max}$), reaction requirements can be reduced to $Da_{in,\min}$, given by Eq.(40). Results for laminar flow inside a circular channel with $Sc = 1$, $\Delta = 0.1$ and $\upsilon = 1.05$.

Figure 12: Performance map for the vertices delimiting the intermediate region. Values of conversion, effectiveness and flow efficiency are normalized by the maximum value observed among the 4 points. Conditions of Figure 6 ($\varepsilon_{fd} = 0.01$, $e_{dev} = 0.01$, $\theta = 0.9$ and $\eta = 0.9$).

TABLES

Table 1: Mass transfer-reaction modeling in wall-coated microreactors.

Table 2: Boundaries for reaction-transport controlling regimes in the $Da_{in} - \alpha\, Pe_m / z - \upsilon - \Delta$ space.

Table 3: Simplified relationships between performance and regime defining criteria.

Figure

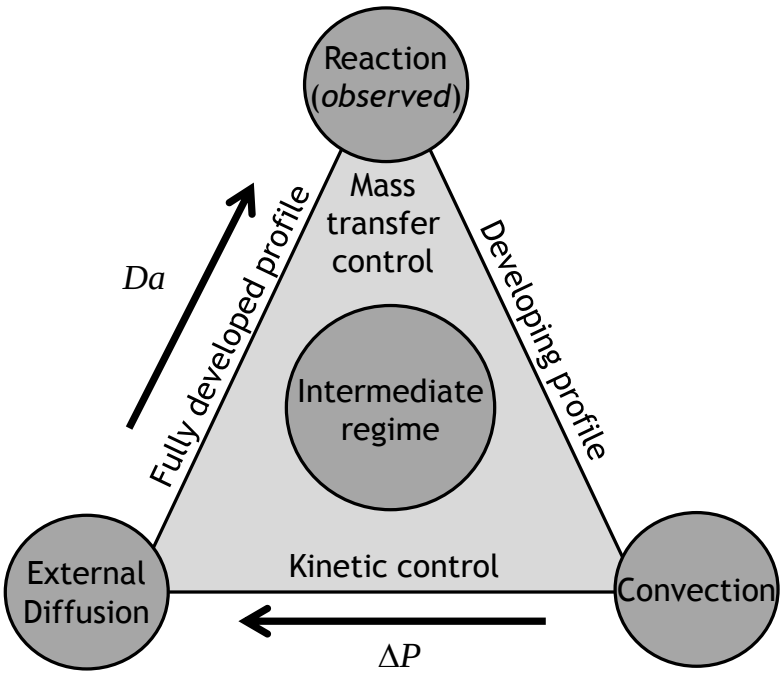

Figure 1

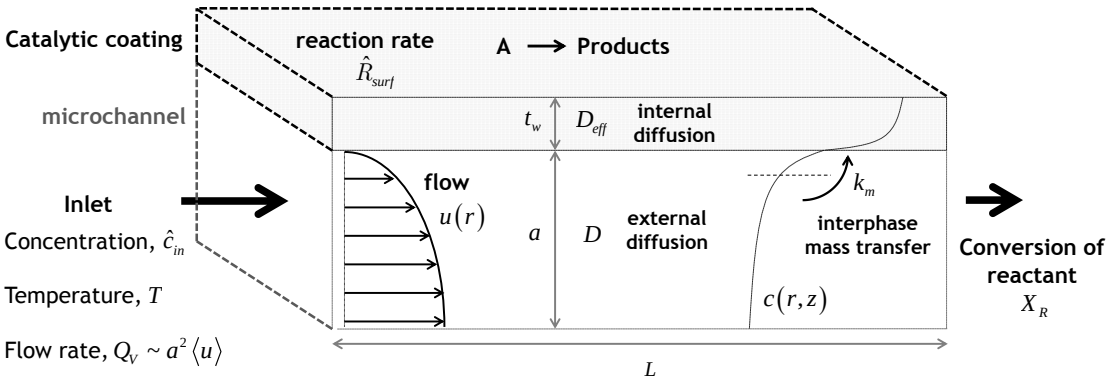

Figure 2

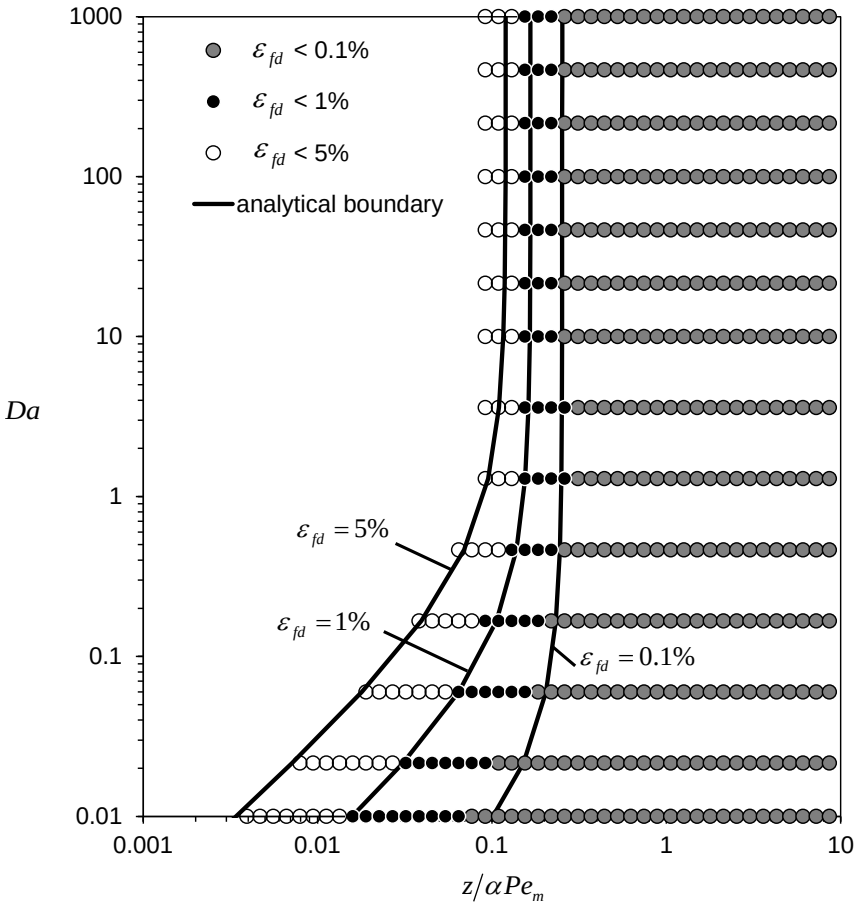

Figure 3(a)

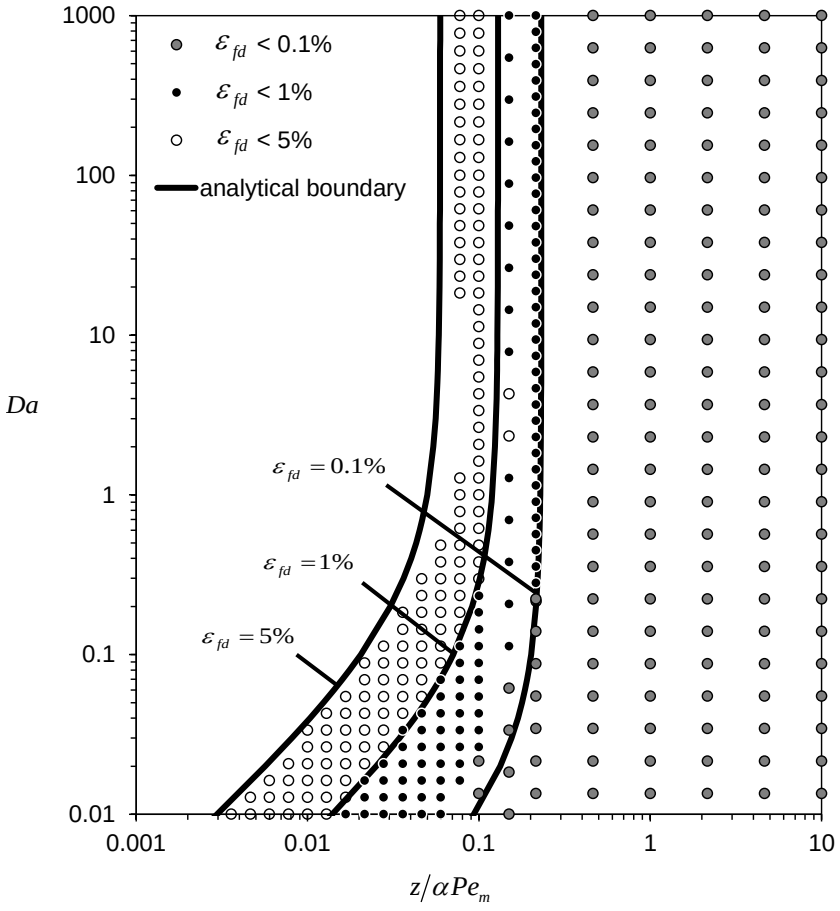

Figure 3 (b)

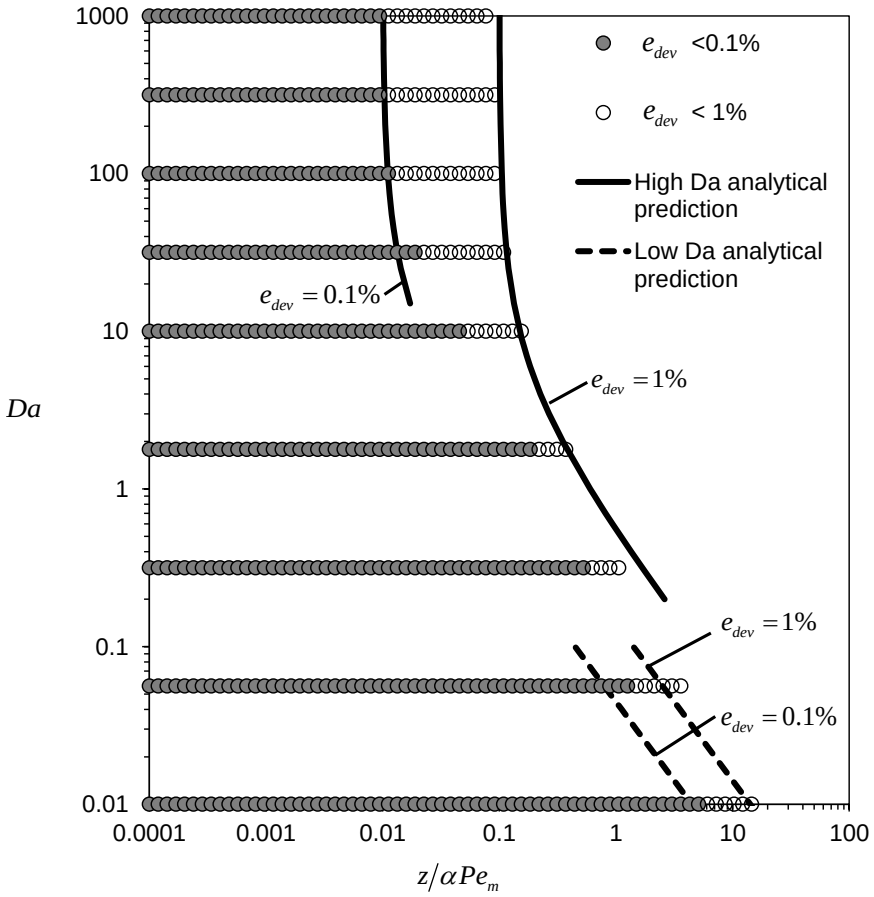

Figure 4 (a)

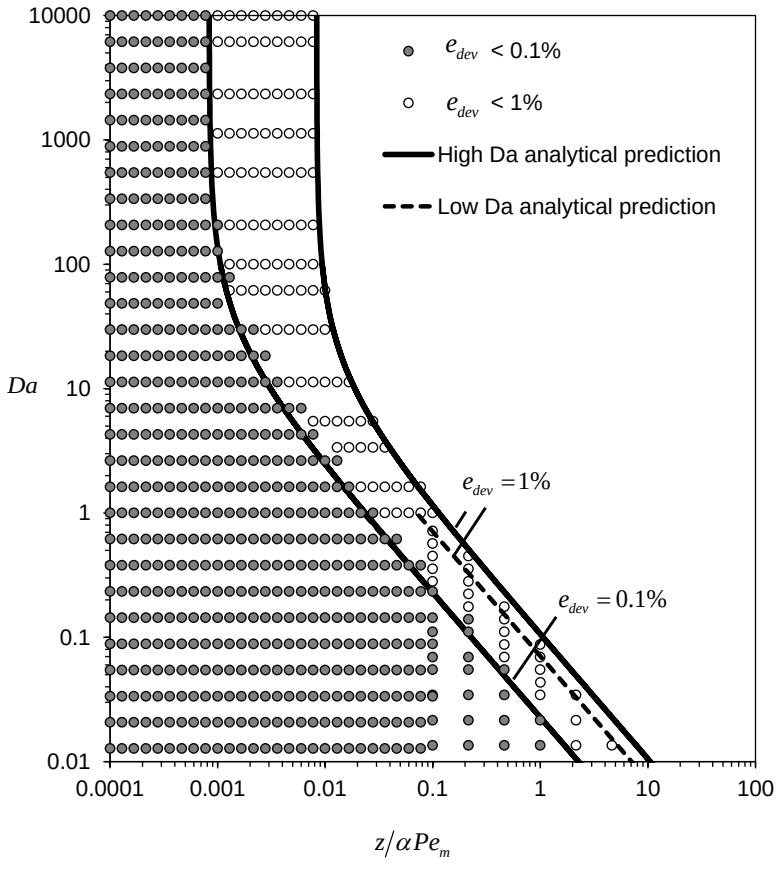

Figure 4 (b)

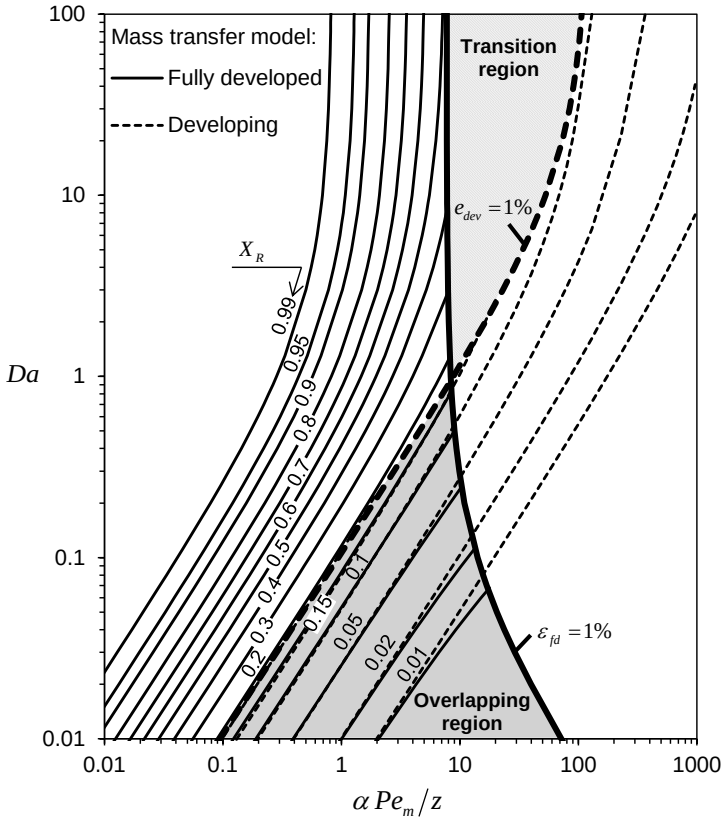

Figure 5 (a)

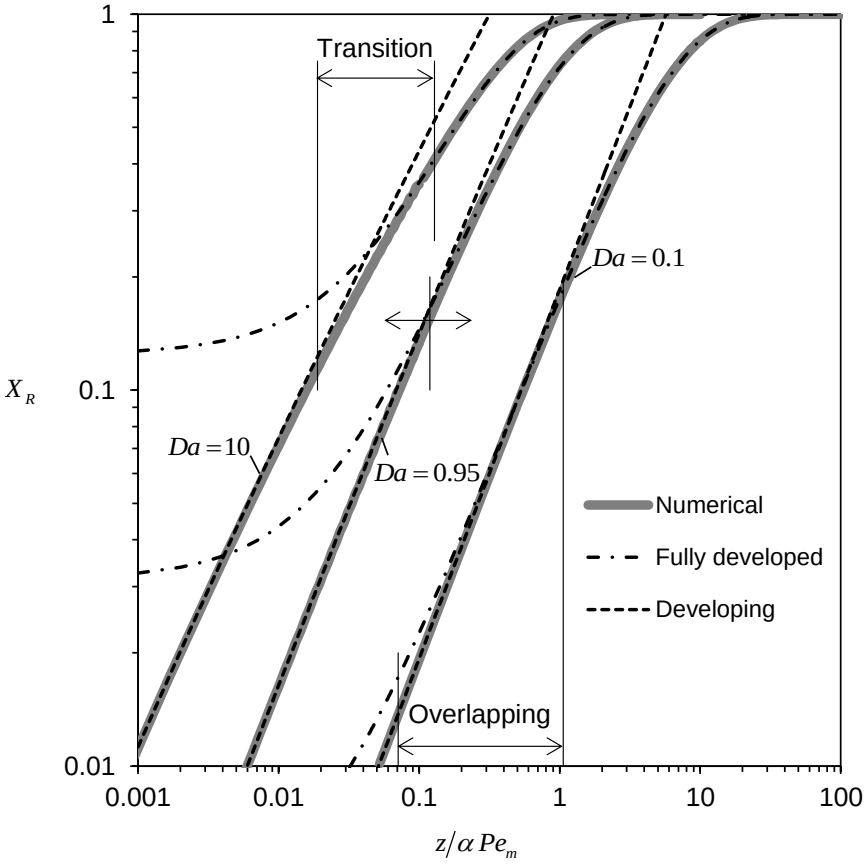

Figure 5(b)

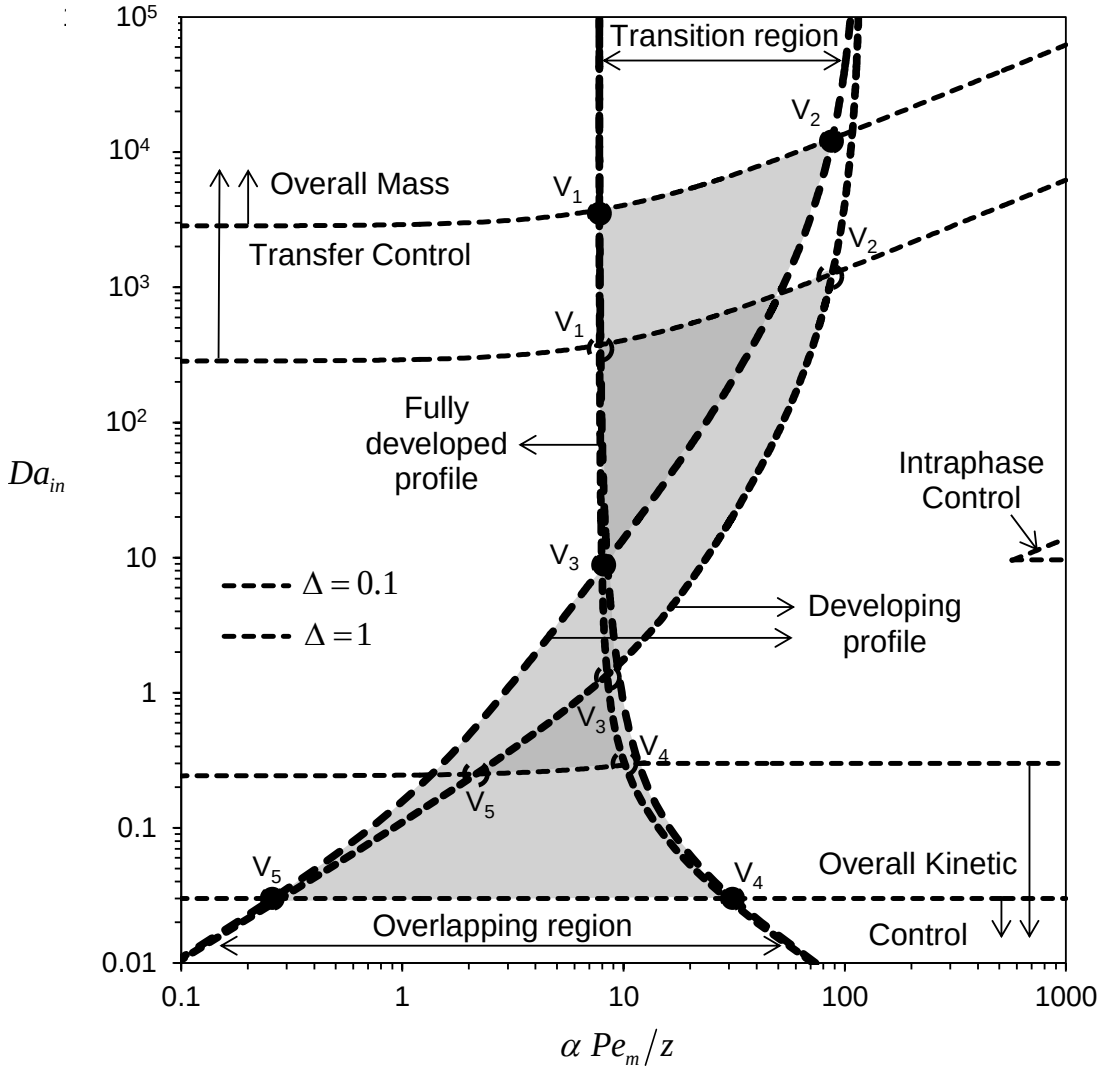
10^5
10^4
10^3
10^2
10
1
0.1
0.01
Da_{in}
0.1
1
10
100
1000
$\alpha\ Pe_m/z$
Transition region
V_2
V_1
Overall Mass
Transfer Control
V_2
V_1
Fully
developed
profile
Intraphase
Control
V_3
$\Delta = 0.1$
$\Delta = 1$
Developing
profile
V_3
V_4
V_5
V_5
V_4
Overall Kinetic
Control
Overlapping region

Figure 6

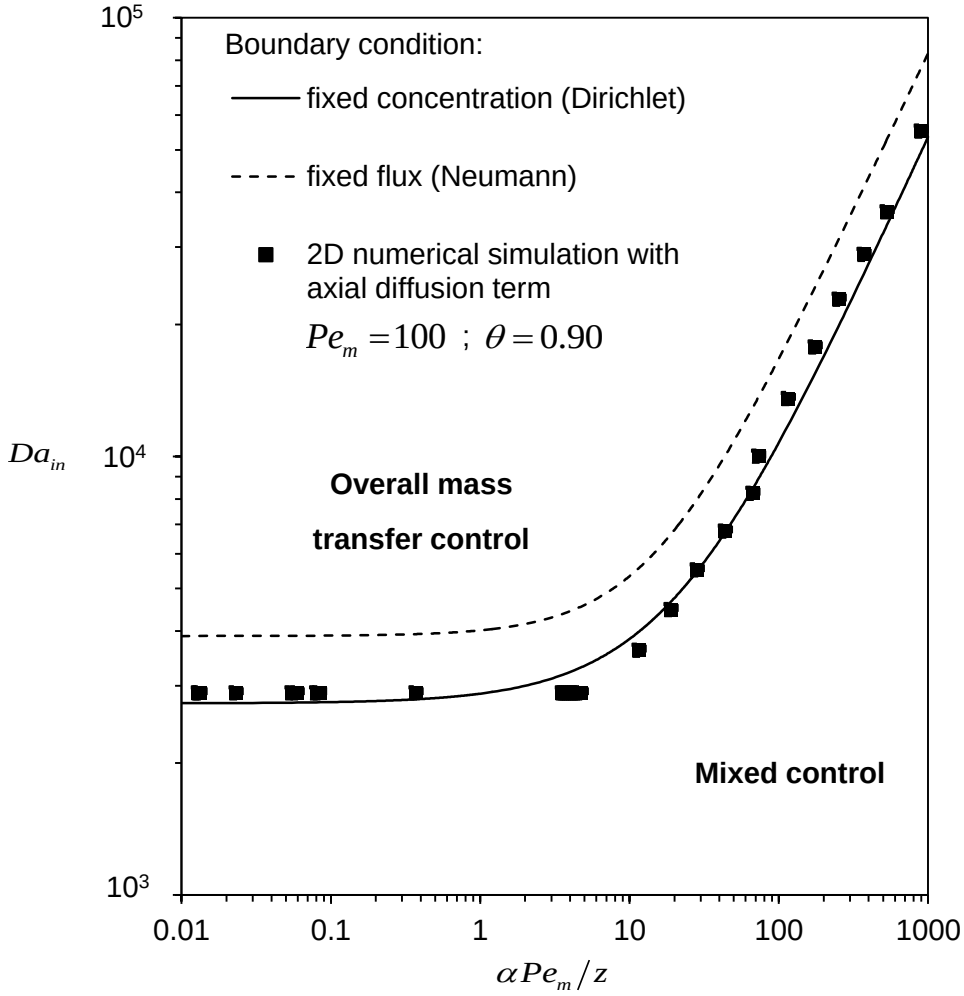
Boundary condition:
fixed concentration (Dirichlet)
fixed flux (Neumann)
2D numerical simulation with axial diffusion term
$Pe_m = 100$; $\theta = 0.90$
Overall mass transfer control
Mixed control
Da_{in}
10^5
10^4
10^3
0.01
0.1
1
10
100
1000
$\alpha Pe_m / z$

Figure 7

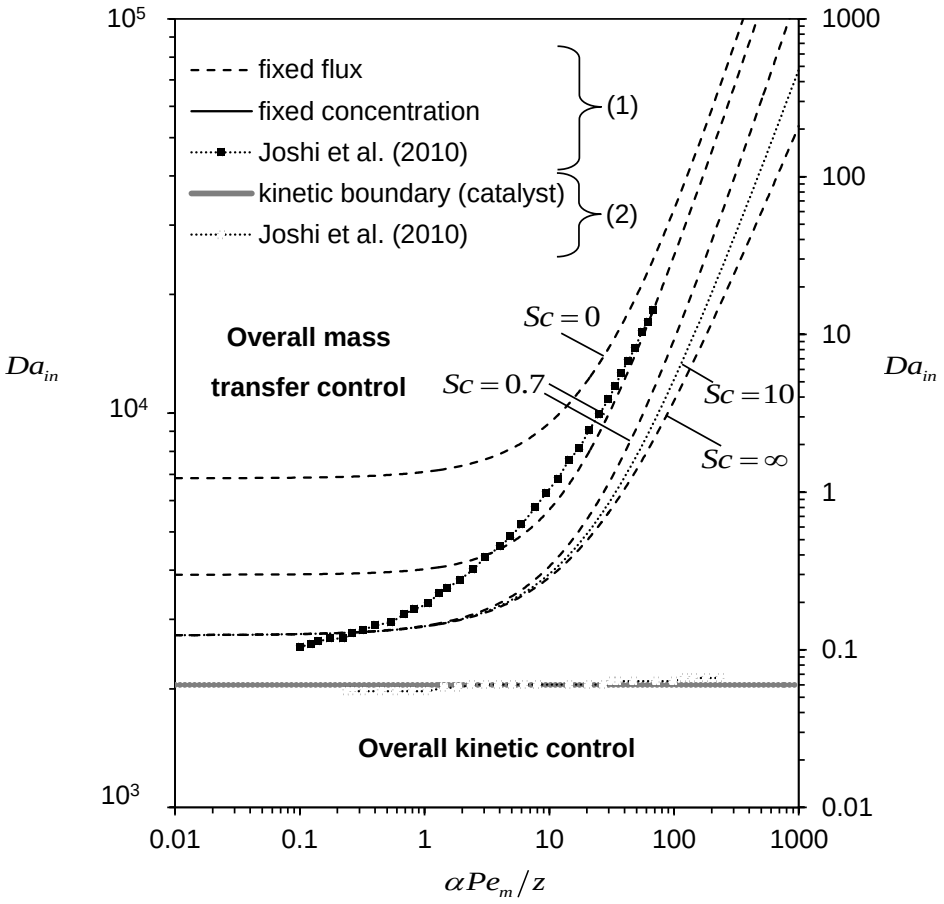
fixed flux
fixed concentration
Joshi et al. (2010)
kinetic boundary (catalyst)
Joshi et al. (2010)
(1)
(2)
Overall mass
transfer control
Sc = 0
Sc = 0.7
Sc = 10
Sc = ∞
Overall kinetic control
Da_in
Da_in
10^5
10^4
10^3
1000
100
10
1
0.1
0.01
0.01
0.1
1
10
100
1000
αPe_m / z

Figure 8

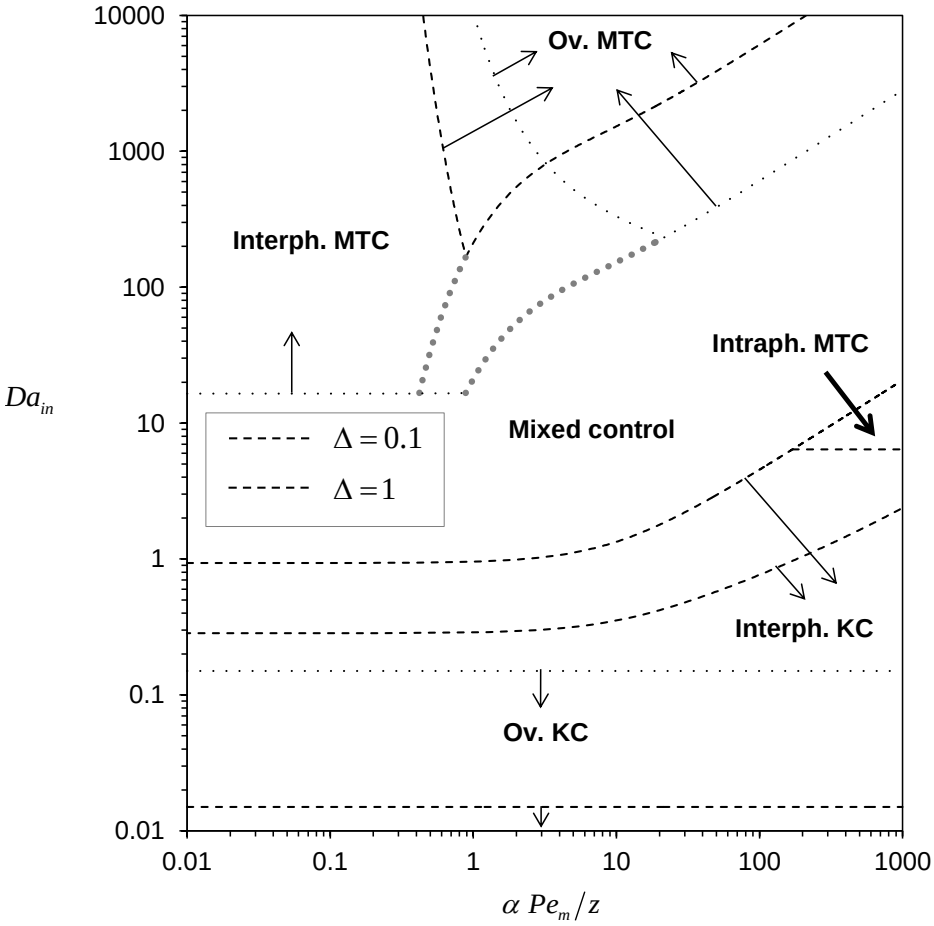
10000
1000
100
10
1
0.1
0.01
0.01
0.1
1
10
100
1000
Da_{in}
$\alpha\ Pe_m/z$
Ov. MTC
Interph. MTC
Intraph. MTC
Mixed control
$\Delta = 0.1$
$\Delta = 1$
Interph. KC
Ov. KC

Figure 9 (a)

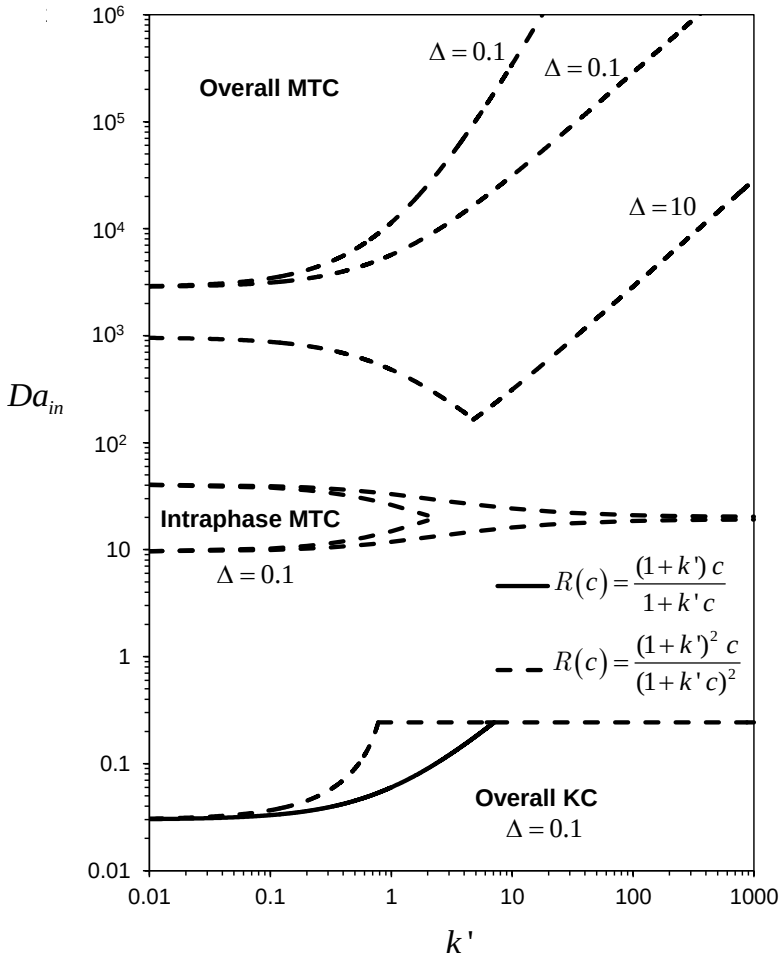
Overall MTC
Δ = 0.1
Δ = 0.1
Δ = 10
Intraphase MTC
Δ = 0.1
R(c) = (1+k')c / (1+k'c)
R(c) = (1+k')² c / (1+k'c)²
Overall KC
Δ = 0.1
Da_in
k'
10⁶
10⁵
10⁴
10³
10²
10
1
0.1
0.01
0.01
0.1
1
10
100
1000

Figure 9 (b)

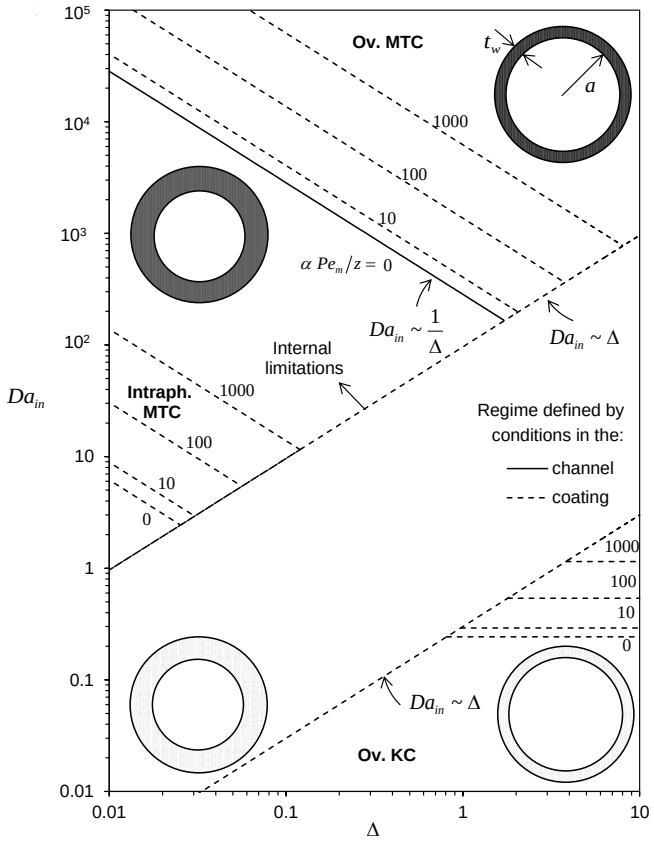

Figure 10 (a)

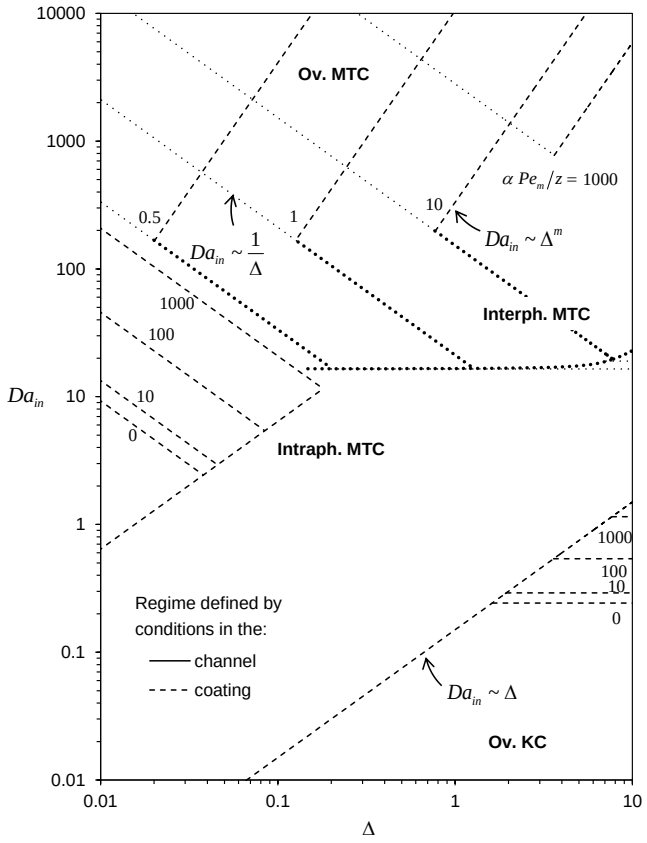

Figure 10 (b)

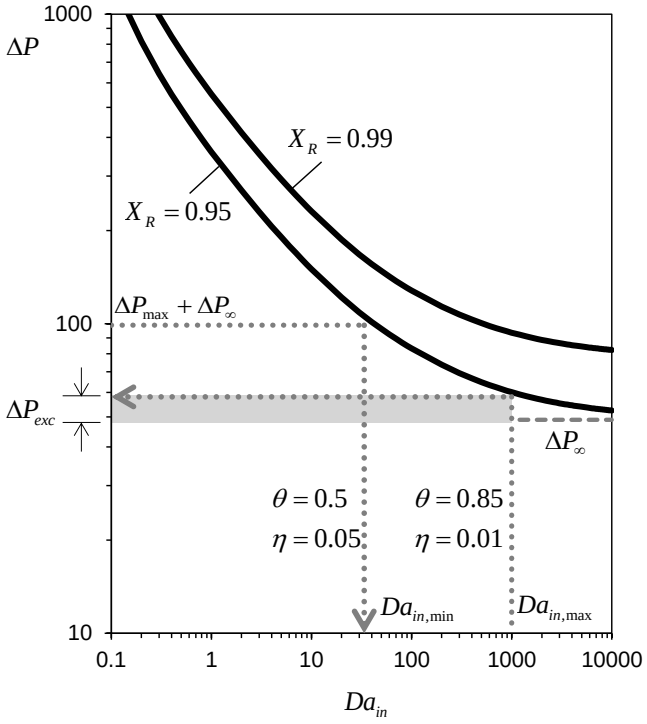

Figure 11

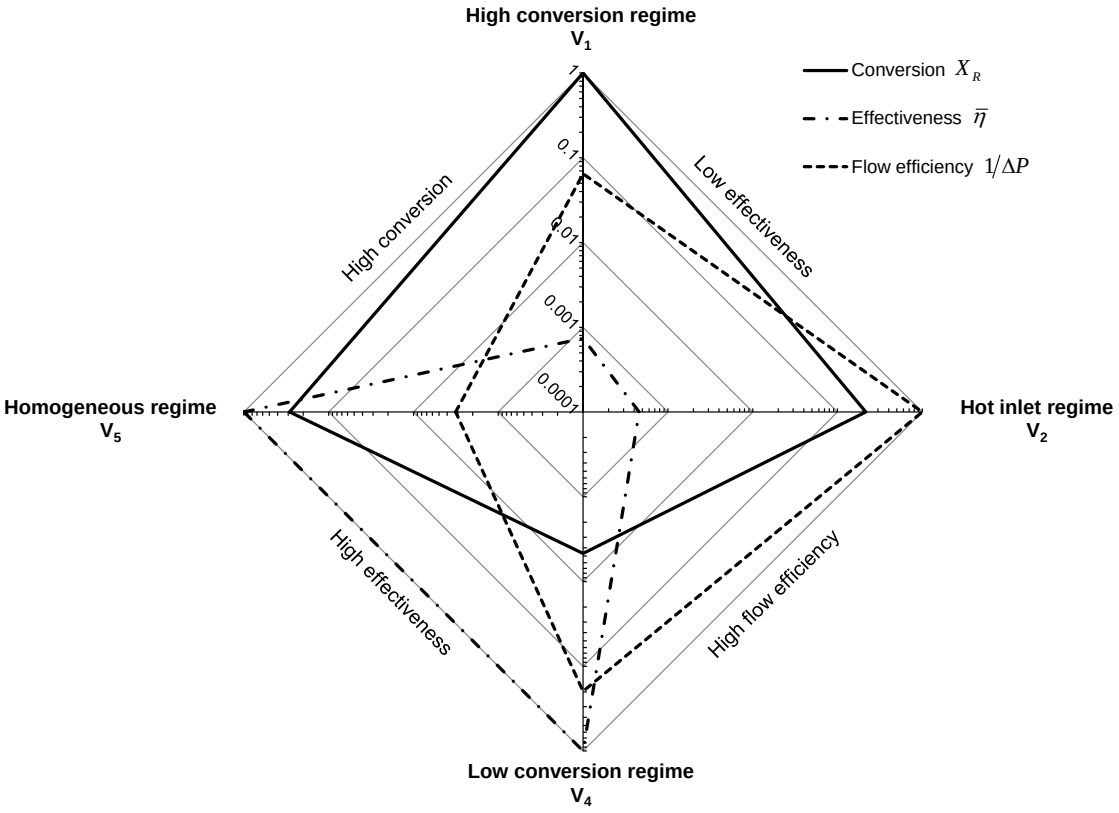

Figure 12

Table

Table 1: Mass transfer-reaction modeling in wall-coated microreactors.

	Regime	Expression	
Conversion	Fully developed profile (valid for all reaction rates)	$X_{fd} = 1 - w_1 \exp\left(\dfrac{-\lambda_1^2 \, z}{\alpha Pe_{m,\max}} \right)$	Approximations for w_1 and λ_1^2 in Lopes et al. (2011b)
	Developing profile (valid for all reaction rates)	$X_{dev} = \dfrac{\sigma_C \, Da \, z/\alpha \, Pe_{m,\max}}{1 + b \, Da \left(z/\alpha \, Pe_{m,\max} \right)^q}$	Lopes et al. (2011b) (laminar flow: $b = 0.9828$; $q = 1/3$)
	Mass transfer control (valid for all Graetz numbers)	$X_R = X_{fd} \, \Theta_{fd} + X_{dev} \, \Theta_{dev}$	Lopes et al. (2012a)
Sherwood number	Fully developed profile	$Sh_{fd} = \lambda_1^2 / \sigma_C$	Shah et al. (1978)
	Developing profile	$Sh_{dev} = M \left(\alpha \, Pe_{m,\max} / z \right)^{1/3}$	Shah et al. (1978)
	$Da_{in} \to 0$	$M = 2^{1/3} / 3^{2/3} \, \Gamma(2/3)$	
	$Da_{in} \to \infty$	$M = 6^{1/3} / \Gamma(1/3)$	
	Correlation (valid for all Graetz numbers)	$Sh = \left[Sh_{fd}^n + Sh_{dev}^n \right]^{1/n}$ ($n = 4$ for laminar flow)	Lopes et al. (2011a)
Effectiveness factor	Thin coatings (valid for all reaction rates)	$\eta = \dfrac{\eta_{slab}}{\upsilon} \left[1 + (\upsilon - 1) \, \eta_{slab} \right]$	Lopes et al. (2012b)
	where,	$\eta_{slab} = \sqrt{\dfrac{\Delta}{\upsilon \, Da_{in}}} \tanh\left(\sqrt{\dfrac{Da_{in}}{\upsilon \, \Delta}} \right)$.	

Table 2: Boundaries for reaction-transport controlling regimes in the $Da_{in} - \alpha\, Pe_m / z - \upsilon - \Delta$ space.

Δ^*	$\Delta < \Delta^*$	$\Delta > \Delta^*$
Overall Kinetic Control (Ov. KC): $\theta \to 0$ and $\eta \to 1$		
$\dfrac{Sh_0\, K_0}{1-\eta}\ \dfrac{\theta}{1-\theta}\ \dfrac{\Lambda}{\upsilon}$ (T1)	$Da_{in} \le \dfrac{\upsilon}{\Lambda}\dfrac{(1-\eta)}{K_0}\Delta$ (T2)	$Da_{in} \le \dfrac{\theta}{1-\theta} Sh_0$ (T3)
Overall Mass Transfer Control (Ov. MTC): $\theta \to 1$ and $\eta \to 0$		
$Sh_\infty \langle c \rangle_\infty^{\frac{m-1}{m}} \dfrac{K_\infty (1+k')^{p/m}\, \upsilon\, \eta}{(1+\upsilon(\upsilon-1)\eta)^{\frac{2m}{m+1}}} \left(\dfrac{\theta}{1-\theta}\right)^{\frac{1}{m}}$ (T4)	$Da_{in} \ge \dfrac{\upsilon\, Sh_\infty^2}{\Delta} K_\infty (1+k')^{p/m} \langle c \rangle_\infty^{1-1/m} \left(\dfrac{\theta}{1-\theta}\right)^{1+1/m}$ (T5)	$Da_{in} \ge \Delta^m \dfrac{(Sh_\infty \langle c \rangle_\infty)^{1-m}}{K_\infty^m (1+k')^p} \dfrac{[1+\upsilon(\upsilon-1)\eta]^{2m}}{\upsilon^m\, \eta^{m+1}}$ (T6)
Intraphase Mass Transfer Control (Intraph. MTC): $\theta \to 0$ and $\eta \to 0$		
$\dfrac{K_\infty\, \upsilon\, \eta}{1+\upsilon(\upsilon-1)\eta} \dfrac{Sh_0\, \theta}{1-\theta}$ (T7)	$Da_{in} \ge \Delta \dfrac{[1+\upsilon(\upsilon-1)\eta]^2}{K_\infty\, \upsilon\, \eta^2}$ (T8) $Da_{in} \le \dfrac{\upsilon K_\infty\, Sh_0^2}{\Delta}\left(\dfrac{\theta}{1-\theta}\right)^2$ (T9)	
Interphase Mass Transfer Control (Interph. MTC): $\theta \to 1$ and $\eta \to \sim 1$		
$Sh_\infty\, \upsilon\, K_\infty (1+k')^{p/m} \langle c \rangle_\infty^{(m-1)/m} \left(\dfrac{\theta}{1-\theta}\right)^{1/m}$ (T10)		$Da_{in} \ge Sh_\infty \dfrac{\theta}{1-\theta}$ (T11)
Kinetic factor (chemical regime)	*Kinetic factor (diffusional regime)*	*Geometry factor*
$K_0 = m - \dfrac{p\, k'}{1+k'}$ (T12)	$K_\infty = \dfrac{(1+k' c_{surf})^{-p}}{2\,\Gamma(1+m)\, {}_2F_1(1+m, p, 2+m, -k' c_{surf})}$ (T13) $K_\infty = \dfrac{m+1}{2}$ (for $c_{surf} \to 0$)	$\Lambda \simeq \upsilon/3$ as $\upsilon \to 1$ (T14)

Table 3: Simplified relationships between performance and regime defining criteria.

Vertex	Criteria	Conversion, X_R	Flow efficiency, $\frac{1}{\Delta P}$	Effectiveness, $\bar{\eta}$
V_1	$\begin{cases}\varepsilon_{fd}\to 0\\ \theta\to 1\end{cases}$	$1-1.1\,\varepsilon_{fd}^{0.16}$	$\frac{0.35}{Sc\left(-\ln\varepsilon_{fd}-1.71\right)}$	$3.35\,\frac{\Delta}{\upsilon}\,\frac{1-1.1\,\varepsilon_{fd}^{0.16}}{-\ln\varepsilon_{fd}-1.71}\left(\frac{1-\theta}{\theta}\right)^2$
V_2	$\begin{cases}e_{dev}\to 0\\ \theta\to 1\end{cases}$	$2.27\,e_{dev}^{2/3}$	$\frac{0.02}{Sc\,e_{dev}}$	$1.65\,\frac{\Delta}{\upsilon}\,e_{dev}^{1/3}\left(\frac{1-\theta}{\theta}\right)^2$
V_4	$\begin{cases}\varepsilon_{fd}\to 0\\ \eta\to 1\end{cases}$	$0.28\,\eta^2\left(1-\eta\right)^2\frac{\Delta^2}{\varepsilon_{fd}}$	$\frac{\varepsilon_{fd}}{3\,Sc\,\Delta\eta\left(1-\eta\right)}$	η
V_5	$\begin{cases}e_{dev}\to 0\\ \eta\to 1\end{cases}$	$\sqrt{2\,e_{dev}}$	$\frac{0.07}{Sc}\,\frac{\Delta\,\eta\left(1-\eta\right)}{\sqrt{e_{dev}}}$	η